2019

Application of Droop Control and Synchronization for Single-Phase Inverters in AC Microgrid Integration

Shuai Yang
Minnesota State University, Mankato

Application of Droop Control and Synchronization for Single-Phase Inverters in AC Microgrid Integration

By

Shuai Yang

Advisor: Dr. Vincent Winstead

A Thesis Submitted to the Graduate School
in Partial Fulfillment of the Requirements
for the Degree of
Master of Science in Electrical Engineering

Minnesota State University, Mankato
Mankato, Minnesota, USA
July 2019

July 9, 2019

Application of Droop Control and Synchronization for Single-Phase Inverters in AC Microgrid Integration

Shuai Yang

This thesis has been reviewed and approved by the following members of the student's examining committee.

_____

Vincent Winstead, PhD, PE

Professor of Electrical and Computer Engineering and Technology

Thesis Advisor and Committee Chair

_____

Xuanhui Wu, PhD

Associate Professor of Electrical and Computer Engineering and Technology

Committee Member

_____

Jianwu Zeng, PhD

Assistant Professor of Electrical and Computer Engineering and Technology

Committee Member

Abstract

With the increasing requirements on environment-friendly and sustainable clean energy [1], people have paid more attention to renewable energy around the world in the past few decades. As a result, power systems have undergone a paradigm shift from centralized generation to distributed generation. Smart grids, which are a combination of power systems and communication networks, were proposed to allow power systems to meet future challenges. In smart grids, especially in AC microgrids, converters play an important role in many areas including microgrid integration, uninterrupted power supply, and flexible alternating current transmission systems.

The inverter is a power conversion device [2] that converts direct current (DC) to alternating current (AC). Among the devices used in AC microgrid integration, the inverter is one of the most important components because it is the ultimate interface between the energy source and the power grid. No matter what type of renewable energy is adopted or what kind of interface structure is employed, an inverter is usually the final step for renewable energy integration. Therefore, an impressive quantity of research has been conducted to the application of inverter in AC microgrid integration.

The most important two aspects regarding the use of inverters are control and synchronization. Droop control is a well-established technique used extensively in power systems ever since synchronous generators were utilized. It has been adopted recently to operate parallel inverters. Since the features between the synchronous generator and the inverter are different, there are some significant difficulties to control the inverter. On the other hand, the well-known phase-locked loop (PLL) is the most common method to get synchronization for an inverter. It has been widely adopted in other areas of modern electrical engineering as well. Typically, the dedicated synchronization unit is regarded as a required item when it comes to the controller, in addition to power, voltage, and current controllers of an inverter. Although extensive investigations have been carried out to improve the performance of PLL, the inherent non-linearity and extensive time commitment for tuning parameters make it still worse when PLL is used for an inverter. This leads to a new question. Can we incorporate the synchronization mechanism into the droop controller? Therefore, the motivation of this thesis is to analyze and solve those issues regarding a combined droop control and synchronization of the inverter.

Acknowledgements

It is my honor to thank many of people who have guided, helped, and encouraged me throughout my graduate school life at Minnesota State University, Mankato (MNSU).

First of all, I would like to express my sincere gratitude to my academic advisor, Dr. Vincent Winstead, for giving me the opportunity to join his renewable energy research team and to attend various professional activities, for helping me to overcome difficulties regarding the changes of my study and research area, and for advising me in many of aspects both academic and in life. Thank you, Dr. Vincent Winstead.

Then, I would like to thank my committee members: Dr. Xuanhui Wu and Dr. Jianwu Zeng. Thanks for their time and effort to become one of my committee members, and for their constructive criticism. I would especially like to thank to Dr. Jianwu Zeng for his professional advice provided in the area of Power Electronics. At the same time, I would also like to thank all faculty and staff from the Department of Electrical and Computer Engineering and Technology (ECET) at MNSU for their work hard, the useful suggestions and comprehensive resources provided to all students.

Next, I would like to thank Dr. J. M. Guerrero and Dr. Q.-C. Zhong. Thanks for their endeavors and fruits on droop control and synchronization of inverters, for their attempts to unify the future power systems, for their works that catalyze the growth process of young professionals.

Finally, I would like to thank my parents and my friends who have always accompanied me with their continuous encouragement and unfailing support.

This accomplishment would not have been possible without any of you. Thank you.

Contents

List of Abbreviations

AC: alternating current

CB: circuit breaker

CDC: conventional droop controller

CG: centralized generation

CVS: controlled voltage source

DC: direct current

DERs: distributed energy resources

DG: distributed generation

ECET: Electrical and Computer Engineering and Technology

EPLL: enhanced phase-locked loop

ESR: equivalent series resistance

ESSs: energy storage systems

IGBT: insulated-gate bipolar transistor

LFAC: line-frequency

LF: loop filter

LHP: left-hand *s*-plan

LPF: low-pass filter

MNSU: Minnesota State University, Mankato

PCC: point of common coupling

PD: phase detection

PLL: phase-locked loop

PWM: pulse-width modulation

P_D: the droop mode of the active power control

P_S: the set mode of the active power control

Q_D: the droop mode of the active power control

Q_S: the set mode of the active power control

RDC: robust droop controller

RMS: the root mean square

STS: static transfer switch

SUDC: self-synchronized universal droop controller

THD: total harmonic distortion

TITO: two-input-two-output

T_C : capacitive transformation matrix

T_L : inductive transformation matrix

T_U : universal transformation matrix

UDC: universal droop controller

VCO: voltage-controlled oscillator

C1.1: case 1 for RDC when the per-unit impedances of two inverters are different

C1.2: case 1 for CDC with same droop coefficients as C1.1

C1.3: case 1 for CDC with different voltage drop coefficient

C2.1: case 2 for RDC when the per-unit impedances of two inverters are same

C2.2: case 2 for CDC with same droop coefficients as C 2.1

C2.3: case 2 for RDC with different proportional coefficient

List of Figures

List of Tables

Chapter 1

Introduction

1.1 Background

There are two ways to produce electricity in the modern electric power system, i.e., centralized generation (CG) and distributed generation (DG). As an approach used in the traditional power system, centralized generation makes use of a few large-scale power stations located far from the load centers. In contrast, distributed generation is an emerging method that employs numerous small-scale technologies to generate electricity close to the end users of power [3]. Their main characteristics are summarized and further compared in Table 1.1.

Item	Centralized Generation	Distributed Generation
Location	Away from consumers	Close to consumers
Scale	Large	Small
Amount	Few	Copious
Capacity	> 100 MW	1 kW – 100 MW
Resources	Coal, oil, and natural gas, etc.	Solar, wind, and tidal, etc.

Table 1.1: Comparison between CG and DG.

There are many of advantages regarding the utilization of distributed generation. Among them, two merits are worth emphasizing. The first one is related to the technical issue caused by the disadvantage of the centralized generation. Although the traditional power grid is continuing to grow worldwide nowadays, the inefficiency of the existing large-scale electrical transmission and distribution network results in inconvenience to many people, especially to the people living in developing countries and rural areas. This problem can be improved dramatically, even be eliminated, by using the distributed generation. The second crucial superiority is reflected in economic cost. Naturally, customers can pay fewer electricity bills so long as a local distributed generation source can provide power. Furthermore, customers even can get income from the electric utility if the generated power locally has the potential to be sold as surplus power back to the grid, especially during the times of peak demand. Therefore, it is the trend that the deployments of distributed generation will continue to increase.

The applications of distributed generation are usually divided into two levels: the local level and the end-point level. Local level power generation plants often use renewable energy technologies, whereas one technology frequently used by the end-point level is the modular internal combustion engine technology [3]. Compared to the end-point level utilizations, the local level applications play a significant part in our current and future life both in the aspects of quantity and quality of electricity generation, so the local level deserves more attention.

1.2 Microgrid Fundamentals

In the context of environmental issues and energy crisis, renewable energy has been widely researched and nearly entirely utilized worldwide in the last few decades due to the environment-friendly character and the nature of replenishment [4]-[7]. At the same time, power system development has gone through several transitions, along with increases in the implementation of renewable energy in the power grid. When the penetration of renewable energy exceeds a certain level, it is unavoidable and necessary that those energy sources will need to participate in the regulation for voltage and frequency of the system. As an interface between renewable energy and the power grid, the inverter plays a vital role in such regulation.

It is common and reasonable that distributed generation and renewable energy form microgrid before they are connected to the utility grid [8]-[10]. A microgrid can be described as a cluster of loads, distributed generation (DG) units and energy storage systems (ESSs) operated in coordination to reliably supply electricity, connected to the host power system at the distribution level at a single point of connection, the point of common coupling (PCC) [6].

There are several ways to identify the type of microgrid. One way is provided by [9]. According to the method used to transmit and distribute the power in the system, microgrids can be classified into three categories: AC microgrids, DC microgrids, and hybrid AC and DC coupled microgrids. AC microgrids can be further divided into two kinds based on the frequency. Compared to others, line-frequency AC (LFAC) microgrids is always the main research area since the microgrid concept was proposed. This is the reason why the focus of this thesis is on AC microgrid, especially for LFAC.

A possible microgrid layout is shown in Fig. 1.1.

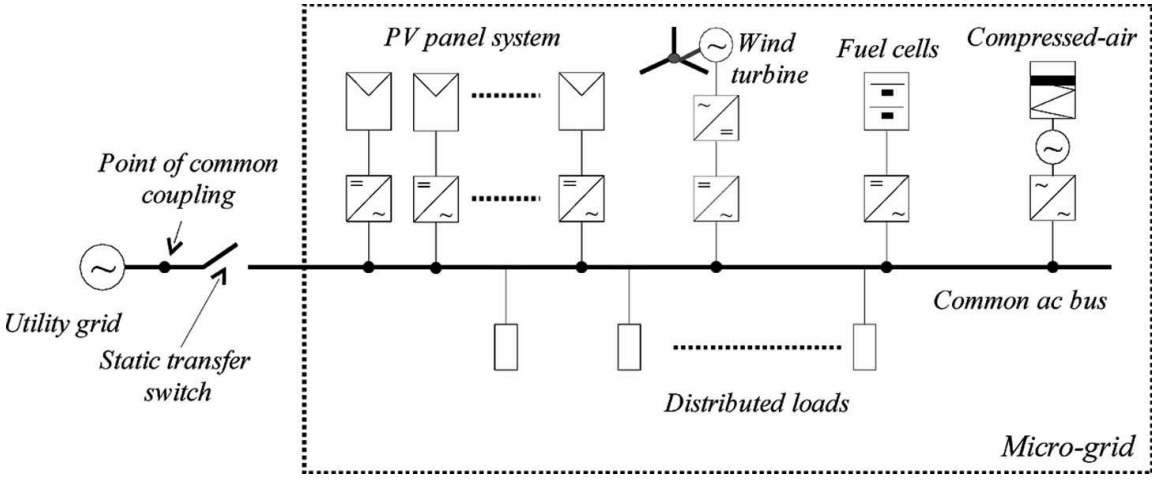

Fig. 1.1: A possible microgrid [13].

This microgrid consists of several distributed energy resources (DERs), distributed loads, and power electronics converters that converter energy and control power flow. A microgrid can be operated in the grid-connected mode through a single PCC by turning on the static transfer switch (STS). A microgrid can also be run in the stand-alone mode when the STS is off.

In the stand-alone mode, the primary control objectives of an inverter are to achieve accurate power sharing among inverters and tight voltage regulation of the grid; in the grid-connected mode, the principal control purpose of an inverter is to regulate power flow between the inverter and the grid [23]. More specifically, the grid-connected mode is divided into two sub-modes, i.e., the set mode and the droop mode. The first one is to send the desired power to the grid; the second sub-mode is to regulate power flow the same as the stand-alone mode according to the changes of voltage and frequency of the grid. For convenience, in this thesis, the set mode is denoted as the P_S mode for the active power and the Q_S mode for the reactive power; the P_D mode and Q_D mode are assigned to the active power and the reactive power in the droop mode, respectively.

Another possible microgrid configuration is shown in Fig. 1.2 after taking communication and importance of loads into consideration.

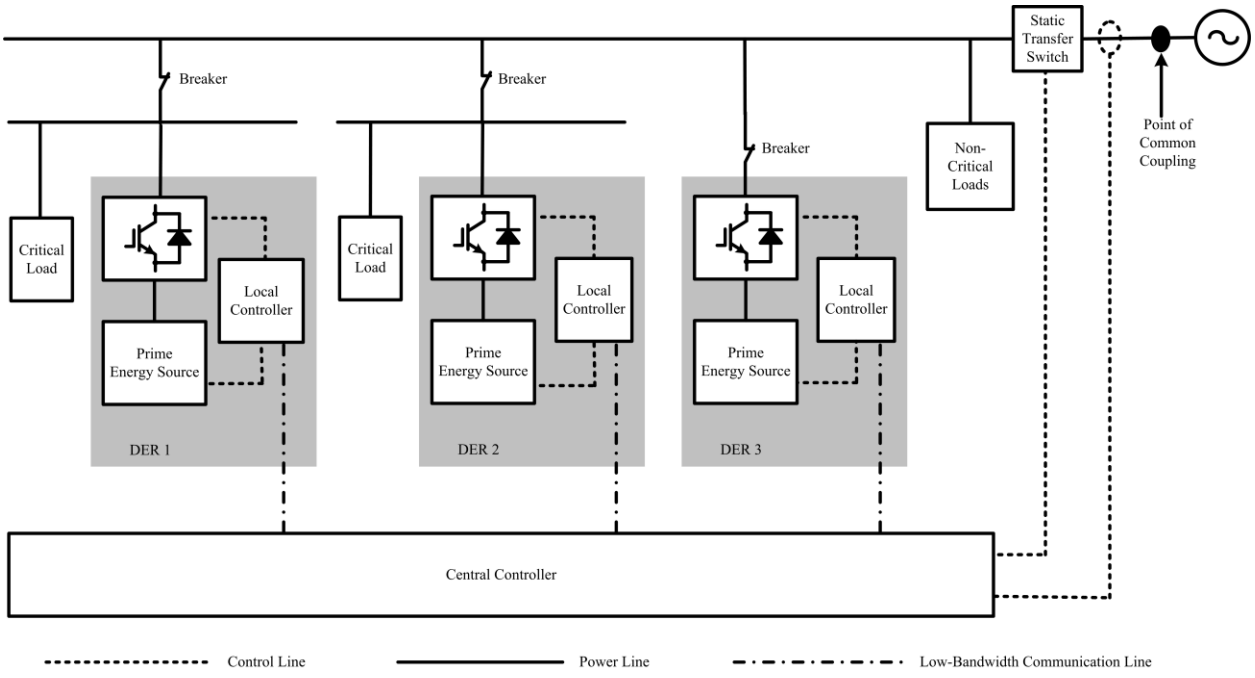

Fig. 1.2: Another possible microgrid [9].

In power systems, droop control has always been a predominant control approach to regulate power flow due to the simple structure itself and the character to be independent of other communication externally [11]-[25]. However, there are different strategies regarding whether to keep conventional characteristics. One group of the researchers, represented by Dr. J. M. Guerrero with his hierarchical control architecture, prefers to adopt an external communication channel to realize sophisticated functionality; Dr. Q.-C. Zhong and Dr. M. Karimi-Ghartemani are the representatives for another group that has focused on the main structure of droop control. We will explore this further.

From the author's point of view, both studies' methods are valuable to finalize the universal architecture, at least for most of the inverters, assuming an increase in the amount of such grid-connected inverters. However, the second one is better if we judge them by the complexity of control structure and simplicity of extensive deployment.

Thus, the goal of this thesis is to analyze, verify, and summarize some of the recent works in the area of control and synchronization for single-phase inverter in AC microgrid integration. The main study materials are [19]-[23]. The accomplishment of this thesis is to describe the relevant theoretical derivation, conduct system modeling and simulation within the MATLAB/Simulink environment, and emphasize two resulting representative simulations with profound analysis.

The rest of this thesis is organized as follows: the theory behind the droop control is first reviewed, then the conventional droop controller (CDC) is designed in Chapter 2. To achieve accurate power sharing and tight voltage regulation, the robust droop controller (RDC) is analyzed in Chapter 3, followed by extending it to more extensive scenarios as the universal droop controller (UDC) in Chapter 4. In Chapter 5, the structural resemblance between the enhanced phase-locked loop and the droop controller is deduced, and the self-synchronization mechanism is explained along with the self-synchronized universal droop controller (SUDC). Finally, conclusions are made in Chapter 6.

Chapter 2

Conventional Droop Controller

2.1 Power Flow Analysis

To illustrate the operational principle of droop control, two parallel inverters are analyzed in this subsection.

As the synchronous generator, an inverter can also be modeled as a voltage source in series with an internal impedance [13]. The model of two parallel-operated inverters is shown in Fig. 2.1.

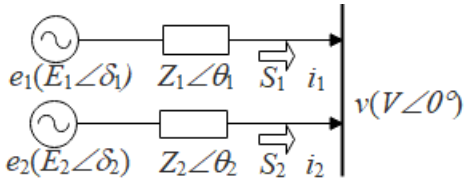

Fig. 2.1: Model of two inverters connected in parallel.

This figure is based on a similar figure from [20].

The internal impedance Z_i of the inverters excludes the line impedances because the internal impedance of the inverters can be designed to dominate the impedance from the inverter to the AC bus [20]. Take the AC bus voltage (terminal voltage, load voltage) as a reference, then the source voltages of the two inverters are

$$e_1 = \sqrt{2}E_1 \sin(\omega_1 t + \delta_1) \tag{2.1}$$

$$e_2 = \sqrt{2}E_2 \sin(\omega_2 t + \delta_2) \tag{2.2}$$

where E_1 and E_2 are the root mean square (RMS) values of the voltage set-points for the inverter 1 and the inverter 2, respectively. Parameters ω_1 and ω_2 are the angular speeds, δ_1 and δ_2 are the initial phases, as known as the power angles.

Because the inverters share the same load, i.e., the AC bus, the load voltages are identical.

$$v = e_1 - Z_1 i_1 = e_2 - Z_2 i_2 \tag{2.3}$$

The equation (2.3) indicates the load effect, and its mechanism is explained as follows. When the load (power) increases at rated inverter output power, the current increases, resulting in the load voltage dropping; conversely, the load voltage boosts when the load decreases.

Fig. 2.1 also includes power delivering. Take the source voltage e_1 and the load voltage v for example and generalize it in the following. The current flowing through the AC bus is

$$i_i = \frac{E_i \angle \delta_i - V \angle 0°}{Z_i \angle \theta_i} \tag{2.4}$$

where θ_i is the impedance angle for the inverter i and V is the RMS value of the load voltage.

The apparent power S_i delivered to the AC bus is

$$\begin{aligned} S_i &= v i_i^* \\ &= V \left(\frac{E_i \cos\delta_i - V + jE_i \sin\delta_i}{Z_i \cos\theta_i + jZ_i \sin\theta_i} \right)^* \\ &= \left(\frac{E_i V \cos\delta_i - V^2}{Z_i} \right) \cos\theta_i + \frac{E_i V \sin\delta_i}{Z_i} \sin\theta_i \\ &\quad + j \left[\left(\frac{E_i V \cos\delta_i - V^2}{Z_i} \right) \sin\theta_i - \frac{E_i V \sin\delta_i}{Z_i} \cos\theta_i \right] \end{aligned} \tag{2.5}$$

Note that the symbol * used in equation (2.5) implies the conjugate value of the current; all others uses of the asterisks in this thesis denote the rated value of the parameter, e.g., S_i^* denotes the rated apparent power for inverter i.

Therefore, the active and reactive power injected into the AC bus are

$$P_i = \left(\frac{E_i V \cos\delta_i - V^2}{Z_i} \right) \cos\theta_i + \frac{E_i V \sin\delta_i}{Z_i} \sin\theta_i \tag{2.6}$$

$$Q_i = \left(\frac{E_i V \cos\delta_i - V^2}{Z_i} \right) \sin\theta_i - \frac{E_i V \sin\delta_i}{Z_i} \cos\theta_i \tag{2.7}$$

2.2 Controller Design Analysis

Generally, the internal impedance of an inverter is inductive [13, 20] due to the large inductor and the highly inductive line impedance caused by the long distance between the units. However, the line impedance is mainly resistive in the low-voltage applications, such as the microgrid. Also, the internal impedance depends on the control strategy as well. It is easy to enforce the internal impedance to be resistive or inductive [11]. It would be better if the internal impedance of an inverter is set as resistive [14] because the resistive impedance is independent of the frequency and the effect of nonlinear loads (current harmonic components) on the voltage total harmonic distortion (THD) is reduced [20]. This is the reason why the following analyses will be conducted for inverters with resistive internal impedance.

The droop control has different forms for different types of internal impedance [13, 26]. For example, compared to the *P*-ω and *Q*-*E* droops used to the inductive internal impedance in traditional power systems, the *P*-*E* and *Q*-ω droops are used when the internal impedance is resistive as in a microgrid.

When the internal impedance is resistive, i.e., $\theta = 0^0$ and $Z_i = R_i$,

$$P_i = \frac{E_i V \cos\delta_i - V^2}{R_i} \tag{2.8}$$

$$Q_i = -\frac{E_i V \sin\delta_i}{R_i} \tag{2.9}$$

If, as is often the case, δ is small enough, i.e., $\sin\delta \cong \delta$ and $\cos\delta \cong 1$, then

$$P_i \cong \frac{E_i V - V^2}{R_i} \tag{2.10}$$

$$Q_i \cong -\frac{E_i V \delta_i}{R_i} \tag{2.11}$$

and the corresponding relation is approximately

$$P_i \sim E_i \tag{2.12}$$

$$Q_i \sim -\delta_i \tag{2.13}$$

Here, the symbol ~ means in proportion to.

As a result, CDC is designed and represented as

$$E_i = E^* - m_i P_i \tag{2.14}$$

$$\omega_i = \omega^* + n_i Q_i \tag{2.15}$$

where E^* is the RMS value of the rated voltage, ω^* is the rated system frequency. Parameters m_i and n_i are the voltage drop coefficient and the frequency boost coefficient, respectively.

The block diagram of the droop controller is drawn in Fig. 2.2.

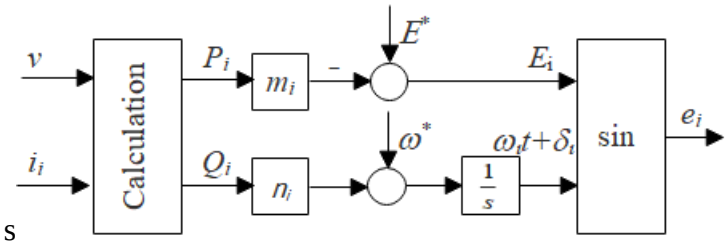

Fig. 2.2: Block diagram of CDC.

This figure is originally from [20] but with modifications from the author.

The mechanisms behind the two equations is illustrated by using the *P*-*E* droop as an example. The active power *P* positively changes when voltage set-point *E* changes according to (2.12). Then, in order to keep *E* tracking the rated value E^*, the voltage control loop works out to this change inversely according to (2.14), which realizes the negative feedback control.

Normally, the voltage drop coefficient m_i and the frequency boost coefficient n_i are determined by the desired voltage drop ratio $\frac{m_i P_i^*}{E^*}$ at the rated active power P_i^* and the desired frequency boost ratio $\frac{n_i Q_i^*}{\omega^*}$ at the rated reactive power Q_i^*, respectively [20].

In order to share the powers to the load in proportion to the power ratings, the inverters are required to set the droop coefficients in inverse proportion to their power ratings [14], that is

$$\frac{m_1}{m_2} = \frac{S_2^*}{S_1^*} = \frac{n_1}{n_2} \tag{2.16}$$

The power ratings of these two inverters are $S_1^* = E^* I_1^*$ and $S_2^* = E^* I_2^*$, where I_i^* is the rated current for inverter *i*.

2.3 Power Sharing Analysis

2.3.1 Active Power Sharing

It is known from [27] that the voltage amplitude deviation of two inverters, i.e., ΔE , results in significant errors to load sharing. To analyze this effect, we need first to derive an expression for ΔE independent on the voltage set-point E_i .

Substituting (2.14) into (2.8), the active power of the inverter *i* is

$$P_i = \frac{E^* \cos\delta_i - V}{m_i \cos\delta_i + \frac{R_i}{V}} \tag{2.17}$$

Substituting (2.17) into (2.14), the voltage amplitude deviation of two inverters is

$$\Delta E = E_2 - E_1 = \frac{E^* \cos\delta_1 - V}{\cos\delta_1 + \frac{R_1}{m_1 V}} - \frac{E^* \cos\delta_2 - V}{\cos\delta_2 + \frac{R_2}{m_2 V}} \tag{2.18}$$

Therefore, in order to achieve accurate proportional load sharing, i.e., $m_1 P_1 = m_2 P_2$ or $\frac{P_1}{S_1^*} = \frac{P_2}{S_2^*}$, ΔE is required to be zero according to (2.14). In practice, ΔE =0 is hard to meet because there are always numerical computational errors, parameter drifts, component mismatches, and disturbances [20]. This strict condition can be satisfied under the following constraints according to (2.18).

$$\begin{cases} \delta_1 = \delta_2 & (2.19) \\ \frac{R_1}{m_1} = \frac{R_2}{m_2} & (2.20) \end{cases}$$

Taking (2.16) into account, we can generate the following relationship between the internal resistors and the power ratings of two inverters.

$$R_1 S_1^* = R_2 S_2^* \tag{2.21}$$

Since the per-unit internal impedance [28] of an inverter is

$$Z_{p.u.,\,i} = \frac{Z_i}{Z_{base}} = \frac{Z_i S_{base}}{V_{base}^2} = \frac{R_i S_i^*}{(E^*)^2} \tag{2.22}$$

Then the equation (2.21) is equivalent to

$$Z_{p.u.,1} = Z_{p.u.,2} \tag{2.23}$$

given E^* is the same for all inverters.

In summary, in order to share the active power accurately in proportion to their power ratings, all parallel-connected inverters equipped with CDC in a microgrid should generate the same voltage set-point E and have the same per-unit internal impedance $Z_{p.u.}$.

2.3.2 Reactive Power Sharing

It is well-known that the inverters synchronize with the utility grid when the systems are stable and have the same frequency as the grid, i.e., $\omega_1 = \omega_2$. This leads to the accuracy of the reactive power sharing of inverters with resistive internal impedances [29].

Then, from (2.15), we have $n_1 Q_1 = n_2 Q_2$ given ω^* is the same for all inverters.

Taking (2.16) into account again, the reactive power sharing in proportion to their power ratings, i.e., $\frac{Q_1}{S_1^*} = \frac{Q_2}{S_2^*}$, is achieved naturally.

Alternatively, using equation (2.9), we have

$$n_1 \frac{E_1 V \sin \delta_1}{R_1} = n_2 \frac{E_2 V \sin \delta_2}{R_2} \tag{2.24}$$

Since $\delta_1 = \delta_2$ in the steady state, the constraints below yield (2.24).

$$\begin{cases} E_1 = E_2 & (2.25) \\ \frac{R_1}{n_1} = \frac{R_2}{n_2} & (2.26) \end{cases}$$

In summary, CDC guarantees the accurate proportional reactive power sharing for the parallel-connected inverters in a microgrid.

Chapter 3

Robust Droop Controller

3.1 Control Strategy Analysis

Because of the inherent limitations when using CDC for the inverter, an improved droop controller [20], also known as RDC, was proposed to achieve accurate proportional load sharing for the parallel-operated inverters in the microgrid. In this subsection, the analysis will be made.

The voltage droop (2.14) can be written in a different way as

$$\Delta E_i = E_i - E^* = -m_i P_i \tag{3.1}$$

Then the voltage set-point E_i can be obtained by integrating ΔE_i

$$E_i = \int_0^t \Delta E_i dt \tag{3.2}$$

This method works for the inverter working in the grid-connected mode because ΔE_i is eventually zero so that the desired power is able to send out to the grid without error, as proposed in [30]-[33]. However, it does not work in the standalone mode because the actual power P_i is determined by the load and the voltage deviation ΔE_i cannot be zero [20]. This is the reason why different controllers were required when an inverter was operated in different modes. It is obvious that a different controller is needed when the mode changes.

On the other hand, the load voltage drop requires adequate attention as the superposition of the load effect (2.3) and the droop effect (2.14) may cause the load voltage to deviate away from to the desired range dramatically. Therefore, there is a need to incorporate the load voltage into a control loop in a way of negative feedback. It can be done by calculating the difference between the rated voltage E^* and the load voltage V then timing this error with a proportional gain k_e, called the voltage coefficient, as a new voltage reference finally comparing with the product $m_i P_i$. This results in the RDC shown in Fig. 3.1.

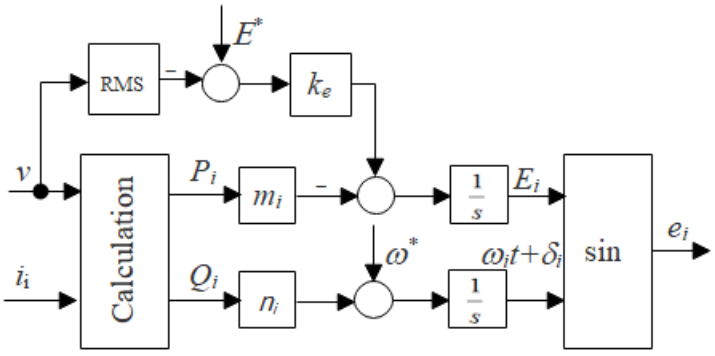

Fig. 3.1: Block diagram of RDC.

This figure is originally from [20] but with modifications from the author.

In the steady state, the input to the integrator in voltage loop should be 0, that is

$$k_e(E^* - V) = m_i P_i \tag{3.3}$$

When k_e is chosen the same for all inverters, the left-hand side of the above Equation is constant, i.e., $m_i P_i = \text{constant}$. It means that the accurate proportional active power sharing is independent of the voltage set-point E_i. Thus, RDC is being more robust to numerical computational errors and disturbances than CDC [20].

Moreover, this strategy attenuates the effect of load voltage drop. The load voltage can be obtained from (3.3)

$$V = E^* - \frac{m_i P_i}{K_e} = E^* - \frac{m_i P_i}{K_e E^*} E^* \tag{3.4}$$

Compared to the conventional voltage drop ratio $\frac{m_i P_i}{E^*}$, the present voltage drop ratio $\frac{m_i P_i}{k_e E^*}$ reduces the voltage drop, which improves the performance strikingly as k_e increases. At the same time, the load voltage drop is determined by the parameters E^*, m_i, P_i, k_e instead of by (2.3).

When we combine equation (3.4) and (3.5), there is a trade-off between the accuracy of active power sharing and the level of voltage drop if there are errors in the RMS voltage measurement. This compromise is because the active power sharing accuracy is inverse proportional to the voltage drop coefficient $\frac{k_e}{m_i}$ but the voltage drop level is proportional to $\frac{k_e}{m_i}$.

Note that more detailed discussions and the theorem of equivalent conditions can refer to [20].

In summary, RDC improves the performance of control theoretically by addressing two issues. One is the inherent limitation of RDC; another is the load voltage drop effects.

3.2 Controller Implementation

Fig. 3.2 shows the circuit diagram of a single-phase inverter, which consists of an insulated-gate bipolar transistor (IGBT) bridge and an LC filter. The inverter is powered by a DC voltage source V_{DC}, controlled by the control signal u_i, and connected to the AC bus through a circuit breaker CB. The load is assumed to be connected to the AC bus.

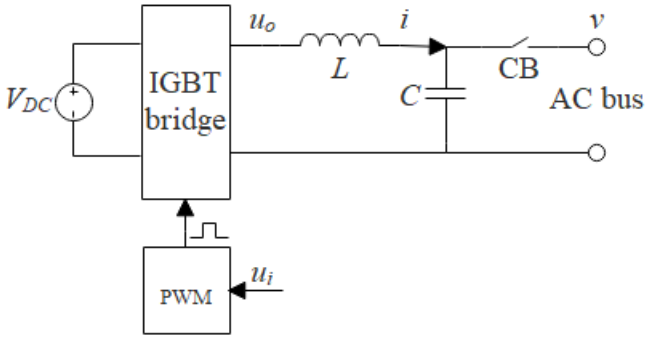

Fig. 3.2: Circuit diagram of single-phase inverter.

This figure is originally from [20] but with modifications from the author.

As shown in Fig. 3.2, the control signal u_i is converted to a pulse-width modulation (PWM) signal to drive the IGBT bridge so that the average of u_o over a switching period is approximate to u_i, i.e., $u_o \approx u_i$ [20].

In order to enforce the internal impedance of the inverter to be resistive [13] and dominate the impedance between the inverter and the AC bus, the inductor current i is measured and then used with a virtual resistor, i.e., R_{vi}, to form an impedance controller shown in Fig. 3.3.

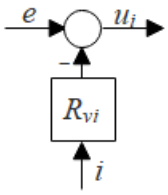

Fig. 3.3: Impedance controller.

This figure is originally from [20] but with modifications from the author.

As a result, Fig. 3.4 shows the integrated controller, i.e., RDC plus impedance controller, of each inverter connected in parallel in a stand-alone microgrid, which compose of an outer composite power sharing and voltage regulation loop, and an inner virtual impedance loop.

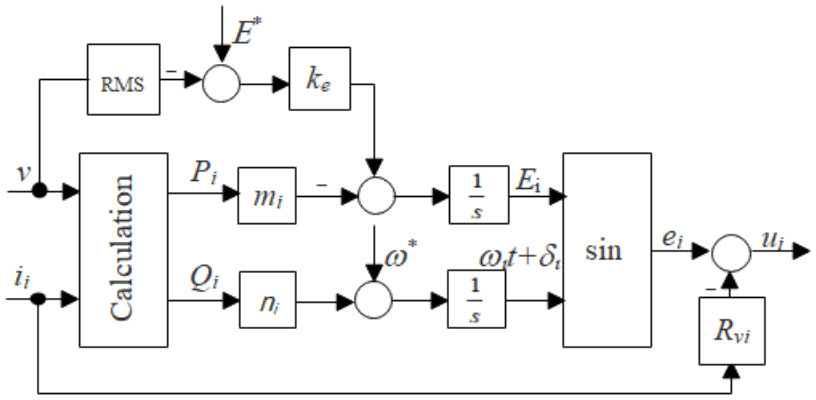

Fig. 3.4: Integrated controller.

From Fig. 3.2 and Fig 3.4, we have

$$u_o = Li_i s + v \text{ when CB is turned on} \tag{3.5}$$

$$u_i = e_i - R_{vi} i_i \tag{3.6}$$

Since $u_o \approx u_i$, there is approximately

$$Li_i s + v = e_i - R_{vi} i_i. \tag{3.7}$$

Then we obtain

$$v = e_i - Z_i i_i \tag{3.8}$$

where

$$Z_i = Ls + R_{vi} \tag{3.9}$$

When we choose a high value of R_i, the internal impedance Z_i is close to pure resistive over a wide range of frequencies, that is

$$Z_i \cong R_{vi} \tag{3.10}$$

Therefore, an inverter can be modeled as a controlled voltage source (CVS) e_i in series with a resistive internal impedance R_{vi}, as described in (2.3) and (3.8).

Note that the capacitor is regarded as a part of the load in RDC, instead of a part of the inverter [20].

3.3 Case Studies

Two typical cases were implemented in the MATLAB/Simulink for verifying functionality of RDC and researching effects of parameter. The simulation parameters are listed in Table 3.1.

Parameter	Value	Unit
V_{DC}	42	V
f	50	Hz
f_s	7.5	kHz
E^*	12	V
ω^*	100π	rad/s
L	2.35	mH
C	22	μF
K_e	10	
m_1	0.4	
n_1	0.1	
m_2	0.8	
n_2	0.2	
R	9	Ω

Table 3.1: Simulation parameters of two inverter equipped with RDC.

These data are original from [20].

where R is a linear resistive load.

Our expectances are that

(1) total (active) power of the load should be around $P = \frac{V^2}{R} = \frac{12^2}{9} = 16\text{W}$;

(2) achieving 2:1 power sharing for the inverter 1 and the inverter 2, i.e., $P_1 = 2P_2$ and $Q_1 = 2Q_2$, because $2m_1 = m_2$ and $2n_1 = n_2$.

3.3.1 Case 1

Case 1 is used to demonstrate the functionality of RDC by setting different per-unit internal impedances to inverters. In order to make the per-unit internal impedances of these two inverters different significantly, virtual internal impedances both were chosen as 14, i.e., R_{v1}=R_{v2}=14.

The simulations were conducted in the following sequences.

(1) at t=0 s, only inverter 2 was connected to the load at the beginning of simulation;

(2) at t=1 s, inverter 1 was connected to the load, two inverters operated in parallel;

(3) at t=8 s, inverter 1 was disconnected from the load;

(4) at t=9 s, stop the simulation.

The simulation results are shown in Fig. 3.5.

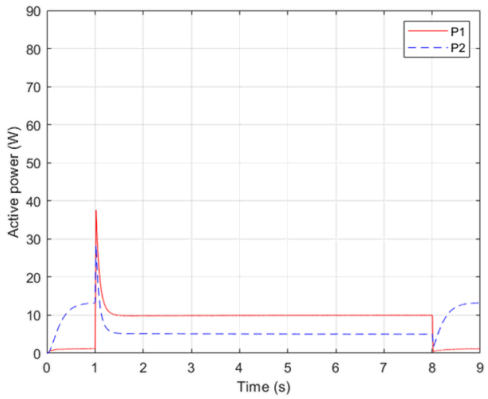

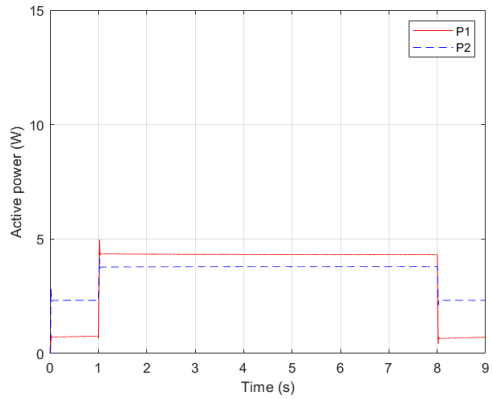

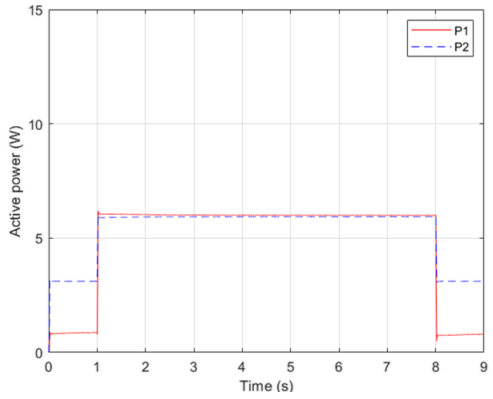

(a) Active power;

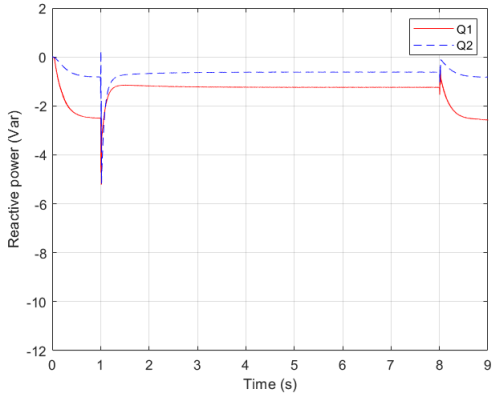

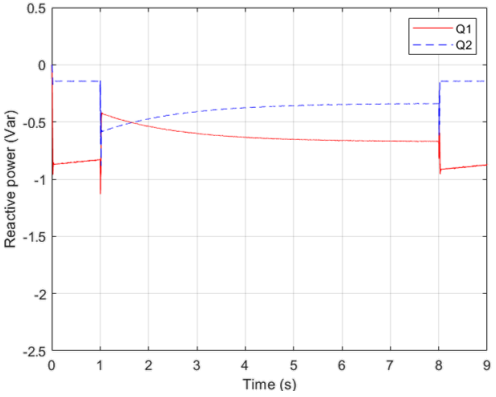

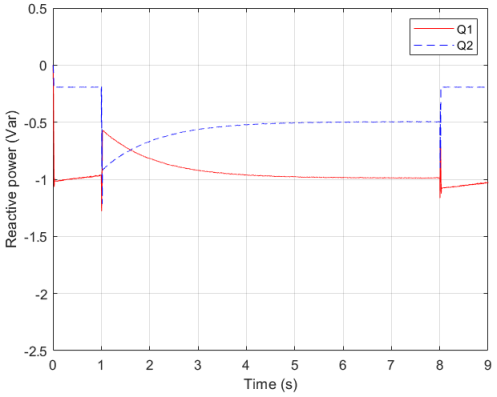

(b) Reactive power;

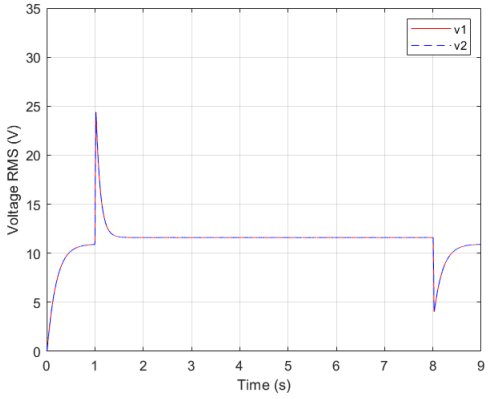

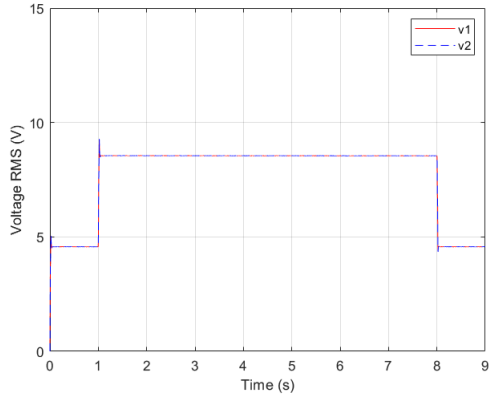

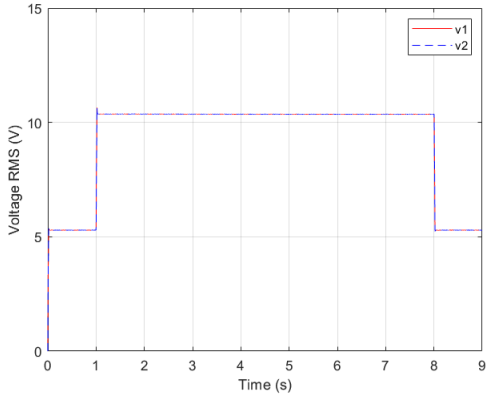

(c) Load voltage;

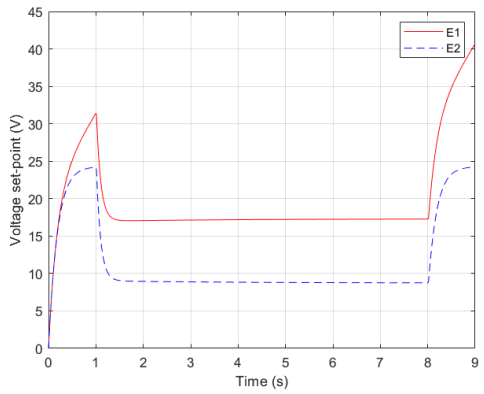

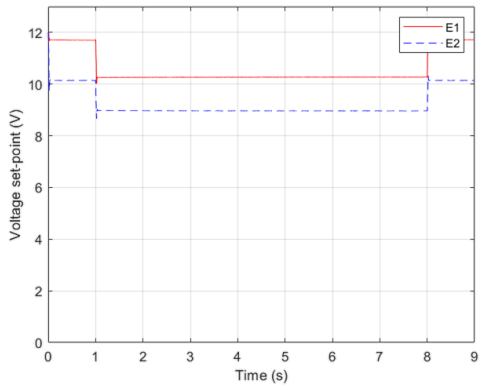

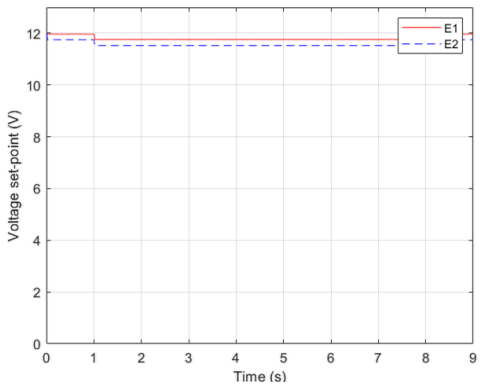

(d) Voltage set-point;

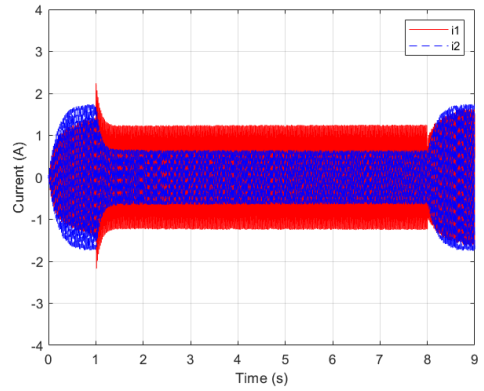

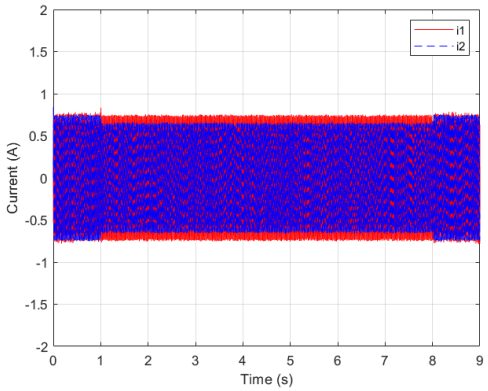

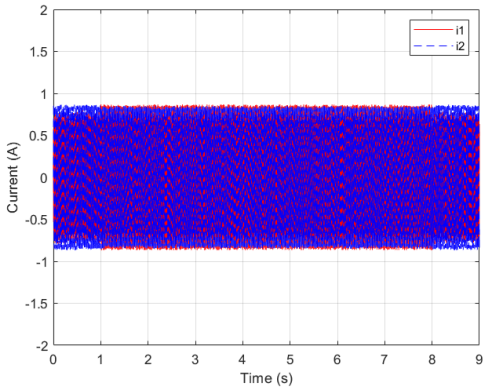

(e) Current;

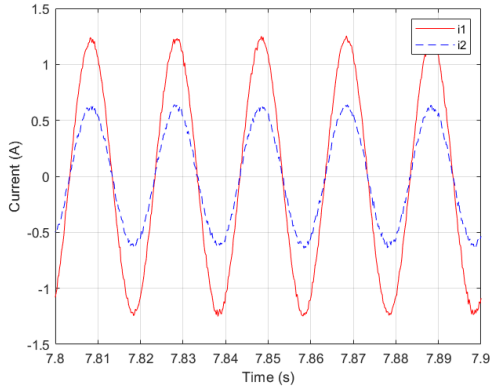

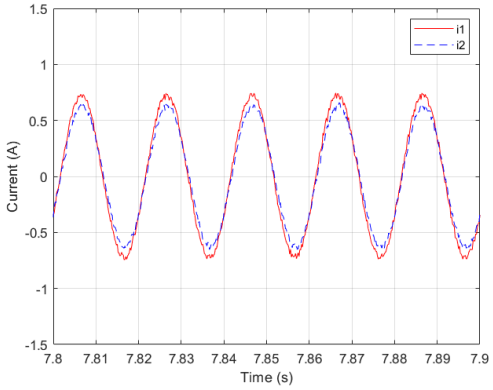

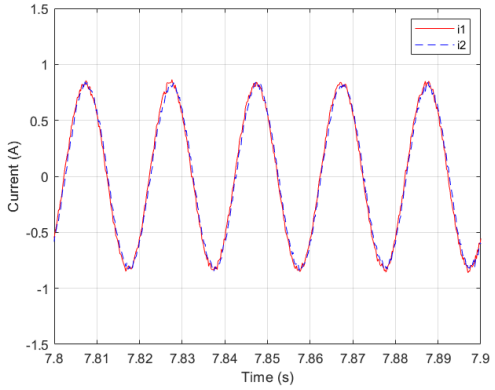

(f) Steady-state current.

Fig. 3.5: Simulation results for case 1.

In Fig. 3.5, the left column shows the results by using RDC with droop coefficients m_1=0.4, n_1=0.1 and m_2=0.8, n_2=0.2, marked as C1.1; the middle column shows the results by using CDC with the same droop coefficients like RDC, noted as C1.2; the right column shows the results by using CDC with the different voltage drop coefficients, i.e., m_1=0.04 and m_2=0.08, to achieve the same equivalent voltage drop ratio as C1.1, specified as C1.3.

In the following results analysis, the steady-state time point is selected at 7.9s.

The active power was shared in the ratio of $\frac{P_1}{P_2}=\frac{9.9597}{5.0063}\cong\frac{1.989}{1}\cong\frac{2}{1}$ for the inverters equipped with RDC in C1.1, which approximately achieve the desired ratio $\frac{2}{1}$. However, the inverters equipped with CDC could not meet our expectation because $\frac{P_1}{P_2}=\frac{4.3266}{3.7978}\cong\frac{1.139}{1}\neq\frac{2}{1}$ and $\frac{P_1}{P_2}=\frac{5.9969}{5.9337}\cong\frac{1.011}{1}\neq\frac{2}{1}$ for C1.2 and C1.3, respectively.

On the other hand, although the values are different, all cases achieved the reactive power sharing in the ratio of 2:1 approximately. Specifically, $\frac{Q_1}{Q_2}=\frac{1.2432}{0.6188}\cong\frac{2.009}{1}\cong\frac{2}{1}$, $\frac{Q_1}{Q_2}=\frac{0.6697}{0.3407}\cong\frac{1.966}{1}\cong\frac{2}{1}$, and $\frac{Q_1}{Q_2}=\frac{0.9871}{0.4958}\cong\frac{1.991}{1}\cong\frac{2}{1}$ for C1.1, C1.2, and C1.3.

From Fig. 3.5 (c), inverter 1 picked up the load, gradually in C1.1, and quickly in C1.2 and C1.3., with different steady voltages, i.e., 11.6007, 8.5464, and 10.3567 for three cases.

Note that the overshoot of the active power is caused by the overshoot of the voltage. There are two possible reasons for voltage overshoot. The first one is that the default parameters of CB were used in the simulation, and this can be improved by optimizing the parameters. The other one results from the impedance controller. Increasing the value of R_{vi} will release this overshoot but slow down the response speed.

When using CDC, the trade-off between the power sharing accuracy and the voltage drop regulation was shown clearly in C1.2 and C1.3. Compared to C1.2, C1.3 achieved tight voltage drop but the active power sharing is worse. In contrast, RDC relaxed this plight considerably and achieved high accuracy of proportional power sharing while controlling small voltage drop.

The mechanism of voltage regulation is hidden at voltage set-point setting. From Fig. 3.5 (d), RDC increased remarkably the voltage set-point. But CDC failed to do this job because the limitation of controller design, that is $E<E^*$ due to $E=E^*-mP$. From Fig. 3.5 (d), we also observed that the set-point for inverters are different. This is because the per-unit internal impedances are different. From Fig. 3.5 (f), the current amplitude indicates the power sharing well when the system is in the steady state. And the currents in all cases were repeated five cycles, i.e., period $T=0.02$s, which means the frequency of inverters are 50 Hz.

3.3.2 Case 2

Case 2 is used to compare the functionality of RDC with CDC and to study the influences of parameter change, i.e., k_e as the variable parameter, when setting same per-unit internal impedances for inverters. To make the per-unit internal impedances of these two inverters equal, virtual internal impedances were chosen in a ratio of 1:2, i.e., R_{v1}=7 and R_{v2}=14.

The simulations were conducted in the same procedures described in case 1.

The simulation results are shown in Fig. 3.6.

In Fig. 3.6, the left column shows the results by using RDC with $k_e = 10$, denoted as C2.1; the middle column shows the results by using CDC with the same coefficients like C2.1, i.e., m_1=0.4, n_1=0.1 and m_2=0.8, n_2=0.2, denoted as C2.2; the right column shows the results by using RDC with the different proportional coefficient k_e, i.e., $k_e = 5$, denoted as C2.3.

Once again, the steady-state time point is chosen at 7.9s.

Observing the C2.1 and C2.2, we can make a comparison. In the steady state, both cases shared the active power in the ratio of 2:1 approximately, i.e., $\frac{P_1}{P_2} = \frac{10.0858}{4.8854} \cong \frac{2.064}{1} \cong \frac{2}{1}$ and $\frac{P_1}{P_2} = \frac{9.2006}{4.5747} \cong \frac{2.011}{1} \cong \frac{2}{1}$ in C2.1 and C2.2, respectively. The reactive power was shared well about 2:1 as well, i.e., $\frac{Q_1}{Q_2} = \frac{1.2291}{0.6323} \cong \frac{1.944}{1} \cong \frac{2}{1}$ in C2.1, and $\frac{Q_1}{Q_2} = \frac{1.1416}{0.5707} \cong \frac{2.0004}{1} \cong \frac{2}{1}$ in C2.2. Moreover, the voltage regulation was achieved in an acceptable range for both cases, i.e., 11.6013 in C2.1 and 11.1282 in C2.2. Then, we can draw a conclusion that the performance of RDC is better than CDC when consider power sharing and voltage regulation simultaneously.

Comparing C2.1 with C2.2, the effect of parameter $k_e = 10$ changing is clear in that the system response increases and the voltage drop decreases as $k_e = 10$ gets larger, where steady-state voltage is 11.2475 in C2.3. After several trials, the range of $k_e = 10$ was obtained as 3.6-125.5 in this set of parameters setting to achieve acceptable voltage regulation, i.e., 11-12.

From the curves of C1.1 and C2.1, the main change happened at the voltage set-point in addition to the change rates of transition point that the inverter 1 was connected to the load.

From the figures of C1.2 and C2.2, the power sharing and the voltage regulation were improved considerably for CDC, which demonstrates the impacts of per-unit internal impedance.

The simulation block diagrams are attached in Appendix A. The future works for this Chapter is to optimize parameters, then to extend RDC into more realistic condition, i.e., 240 V with 60 Hz.

In summary, an inverter equipped with RDC can achieve accurate proportional power sharing without the need of having the same per-unit internal impedance. Moreover, the load voltage drop due to the load effect and droop effect is reduced significantly by using RDC.

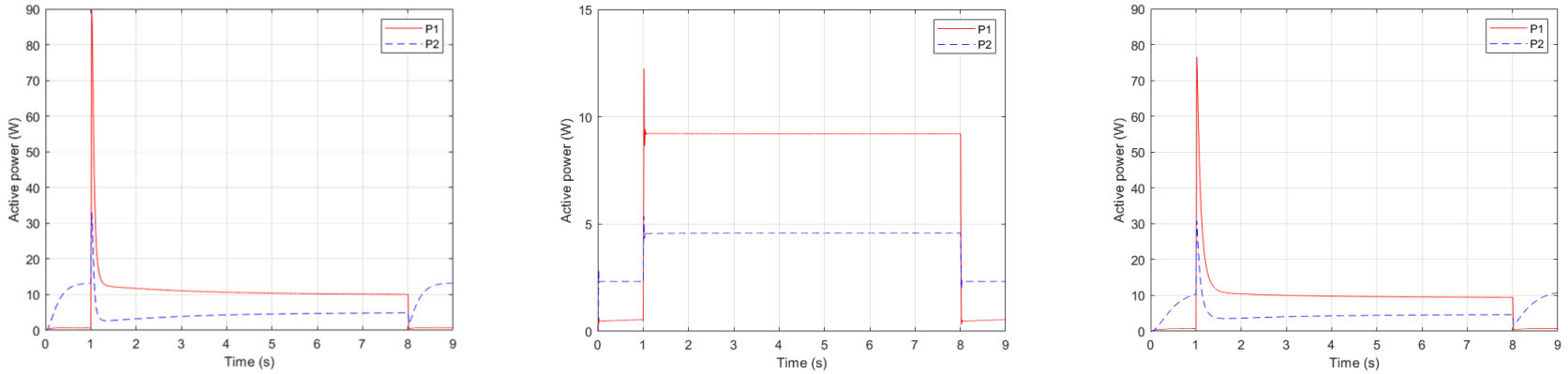

(a) Active power;

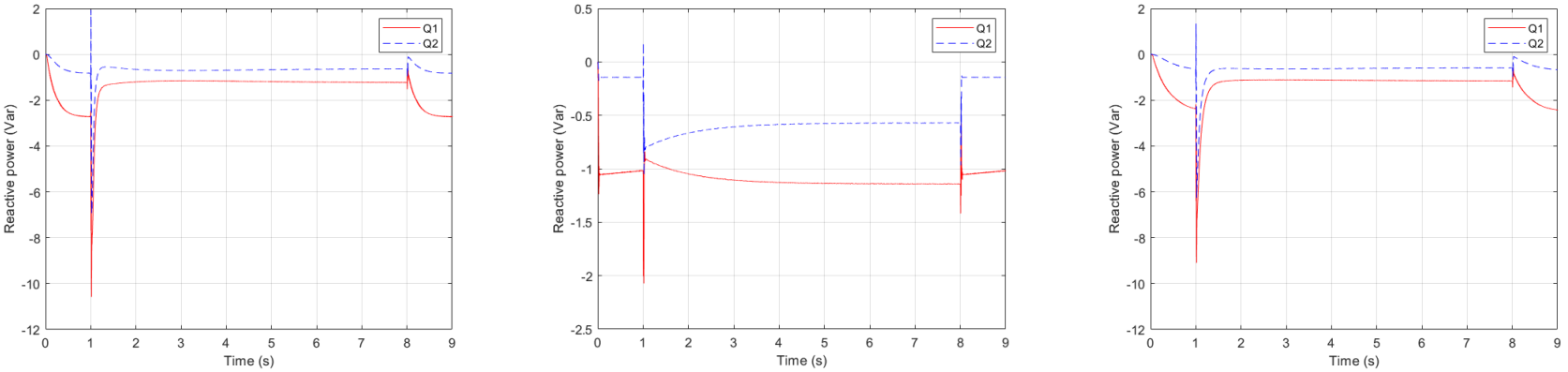

(b) Reactive power;

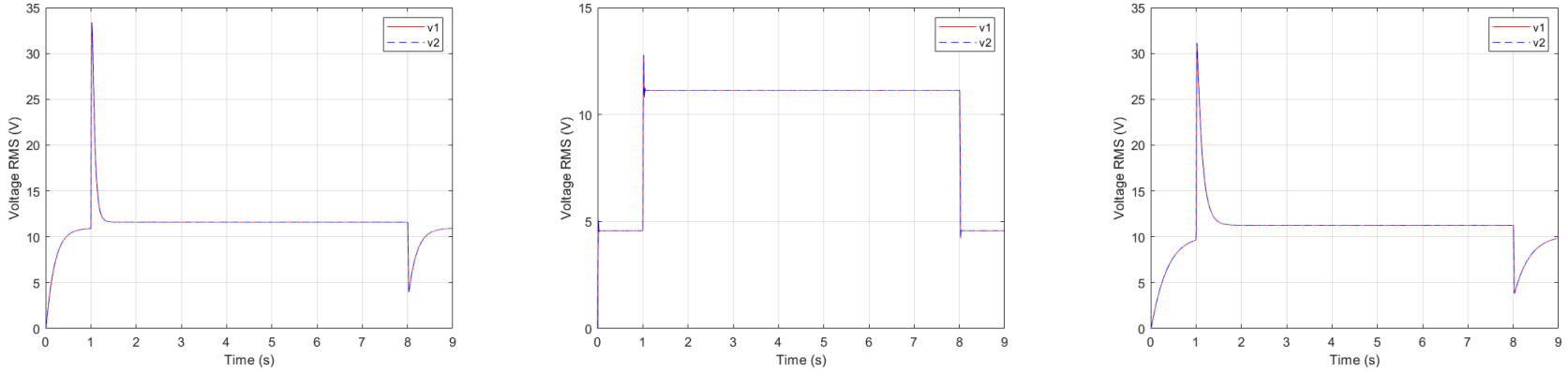

(c) Load voltage;

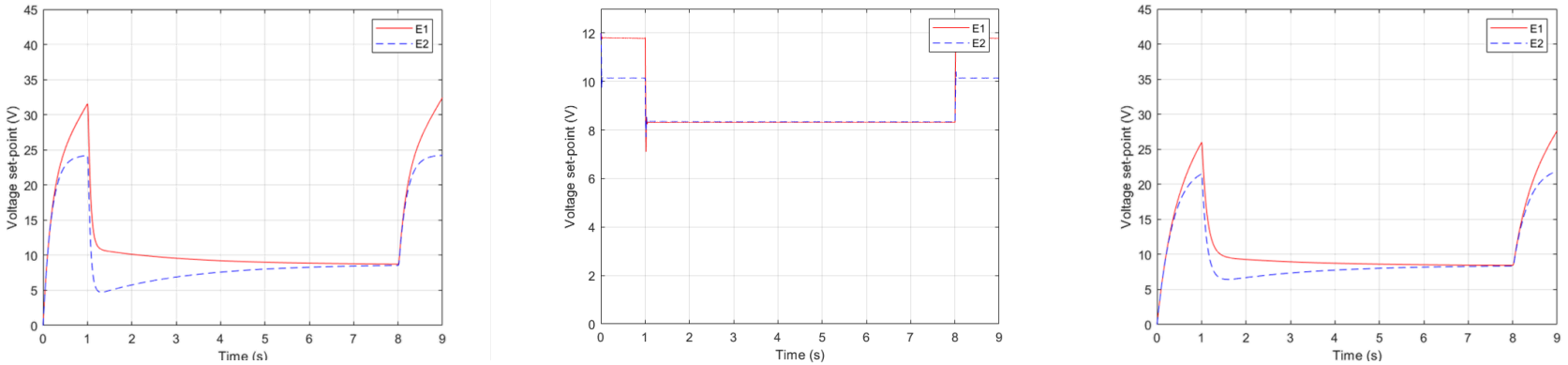

(d) Voltage set-point;

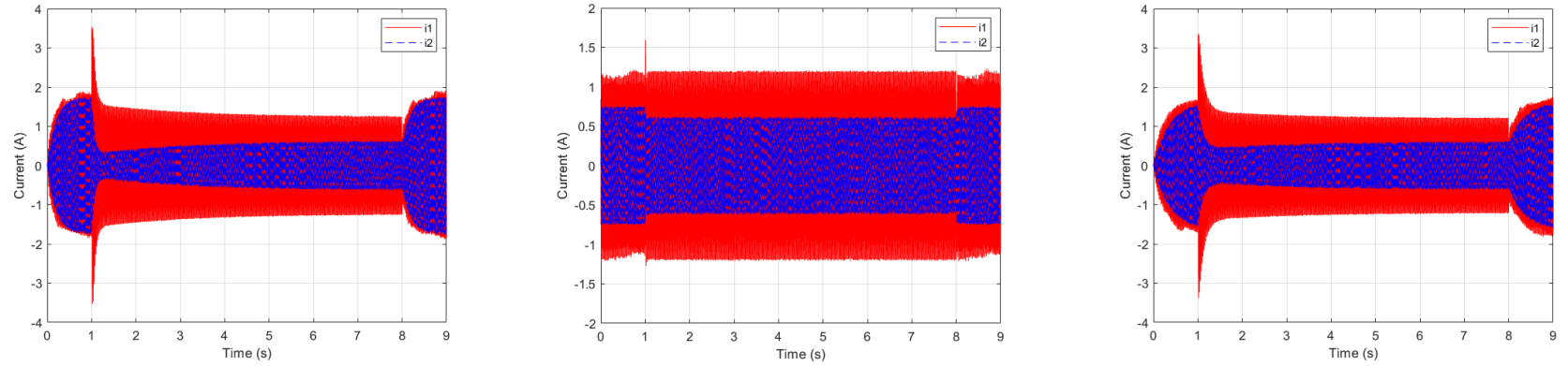

(e) Current;

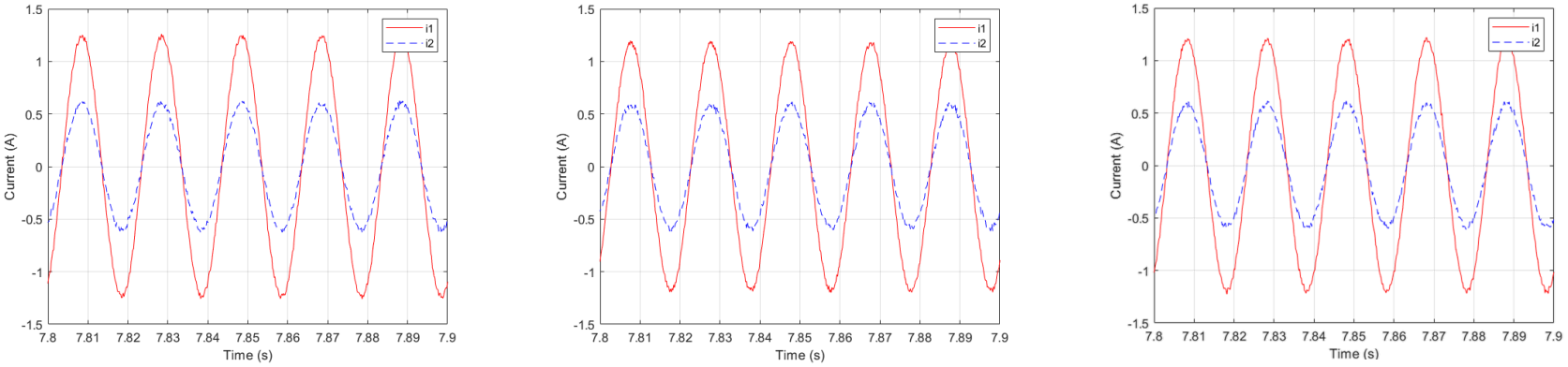

(f) Steady-state current.

Fig. 3.6: Simulation results for case 2.

Chapter 4

Universal Droop Controller

4.1 Control Techniques Review

As analyzed in the preceding two chapters, a single-phase inverter can be modeled as a voltage source with the internal impedance as shown in Fig. 2.1 and redrawn Fig. 4.1.

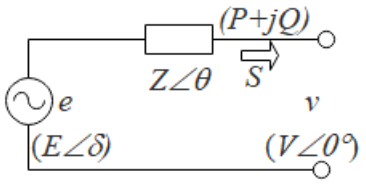

Fig. 4.1: Model of single-phase inverter.

This figure is originally from [21] but with modifications from the author.

The power delivered from the power supply to the terminal load through the internal impedance is described by (2.5) and is rewritten in the form of active power and reactive power as follows:

$$P = \left(\frac{EV\cos\delta - V^2}{Z} \right) \cos\theta + \frac{EV\sin\delta}{Z} \sin\theta \tag{4.1}$$

$$Q = \left(\frac{EV\cos\delta - V^2}{Z} \right) \sin\theta - \frac{EV\sin\delta}{Z} \cos\theta \tag{4.2}$$

From a control perspective, this relationship of the plant between the output power, i.e., P and Q, and the input voltage, i.e., E and δ (ω), is used to build the controller and the block diagram of the closed-loop feedback system is drawn in the following.

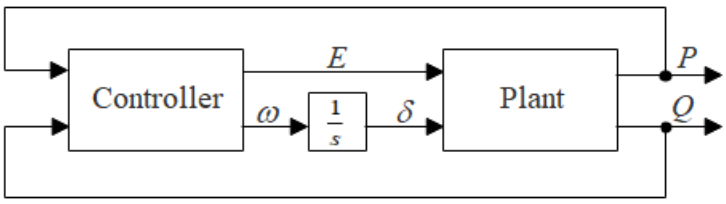

Fig. 4.2: Closed-loop feedback system of single-phase inverter.

This figure is originally from [21] but with modifications from the author.

As we can see from Fig. 4.2, the plant is a two-input-two-output (TITO) system: the inputs are the amplitude E and the phase δ of the voltage source, and the outputs are the active power P and the reactive power Q delivered to the load; the droop controller is used to generate E and δ, which is obtained by integrating the angular speed ω, for the inverter according to the measured power P and Q.

In practice, the power angle δ is small enough so that

$$P \cong \left(\frac{EV - V^2}{Z} \right) \cos\theta + \frac{EV\delta}{Z} \sin\theta \tag{4.3}$$

$$Q \cong \left(\frac{EV - V^2}{Z} \right) \sin\theta - \frac{EV\delta}{Z} \cos\theta \tag{4.4}$$

Take the traditional power systems for example. The internal impedance is assumed to be inductive, then

$$P \cong \frac{EV\delta}{Z} \tag{4.5}$$

$$Q \cong \frac{EV - V^2}{Z} \tag{4.6}$$

Therefore P and Q are roughly proportional to δ and E, respectively.

$$P \sim \delta \tag{4.7}$$

$$Q \sim E \tag{4.8}$$

The traditional droop strategy works by dropping the frequency when the active power increases and dropping the voltage when the reactive power increases.

Similarly, the relationship and the controller design can be analyzed in the cases of the resistive impedance, the capacitive impedance, as well as the coupled situations. Here, the comprehensive summaries are made in Table 4.1.

Inverter type	Impedance angle	Input-output relationship	Droop controller
R	0	$P \sim E$ $Q \sim -\delta$	$E = E^* - mP$ $\omega = \omega^* + nQ$
L	$\frac{\pi}{2}$	$P \sim \delta$ $Q \sim E$	$E = E^* - mQ$ $\omega = \omega^* - nP$
C	$-\frac{\pi}{2}$	$P \sim -\delta$ $Q \sim -E$	$E = E^* + mQ$ $\omega = \omega^* + nP$
RL	$\left(0, \frac{\pi}{2}\right)$	Coupled	Depends on θ
RC	$\left(-\frac{\pi}{2}, 0\right)$	Coupled	Depends on θ

Table 4.1: Droop control techniques for different types of inverters.

This table is originally from [21] but with modifications from the author.

As we can see from Table 4.1, the droop controller changes its form corresponding to the different types of the inverter. There is no way to operate inverters with different types of internal impedance in parallel. For instance, the control strategies are totally opposite to each other when an L inverter and a C inverter are connected in parallel.

4.2 Power Transformation Analysis

4.2.1 RL Controller Analysis

In the literature, some works have been done in the case of R, L, and RL inverters [35]-[36] to study the parallel operation of inverters with different types of internal impedance.

These researches were related to a power transformation. An orthogonal transformation matrix, i.e., the inductive transformation matrix T_L, was introduced as

$$T_L = \begin{bmatrix} \sin\theta & -\cos\theta \\ \cos\theta & \sin\theta \end{bmatrix} \tag{4.9}$$

It transforms the matrix of generic power (4.1), (4.2) into the matrix of specific power when the impedance angle $\theta \in \left(0, \frac{\pi}{2}\right]$.

$$\begin{bmatrix} P_L \\ Q_L \end{bmatrix} = T_L \begin{bmatrix} P \\ Q \end{bmatrix} = \begin{bmatrix} \frac{EV\sin\delta}{Z} \\ \frac{EV\cos\delta - V^2}{Z} \end{bmatrix} \tag{4.10}$$

This power transformation (4.10) can also be written in the phasor diagram as

$$\begin{aligned} P_L + jQ_L &= \left(P\sin\theta - Q\cos\theta\right) + j\left(P\cos\theta + Q\sin\theta\right) \\ &= \left(\sin\theta + j\cos\theta\right)\left(P + jQ\right) \\ &= \left(\cos\left(\frac{\pi}{2} - \theta\right) + j\sin\left(\frac{\pi}{2} - \theta\right)\right)\left(P + jQ\right) \\ &= e^{j\left(\frac{\pi}{2} - \theta\right)}\left(P + jQ\right) \end{aligned} \tag{4.11}$$

where $j = \sqrt{-1}$.

In other words, the transformation matrix T_L rotates the power vector $P + jQ$ by $\frac{\pi}{2} - \theta$ rad onto the axis aligned with the L inverter [21], as shown in Fig. 4.3.

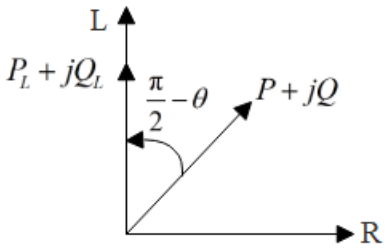

Fig. 4.3: Power transformation by matrix T_L.

This figure is originally from [21] but with modifications from the author.

Because the power angle δ is small enough in power systems, we have roughly

$$P_L \sim \delta \tag{4.12}$$

$$Q_L \sim E \tag{4.13}$$

then the droop controller takes the form of

$$E = E^* - m_L Q_L \tag{4.14}$$

$$\omega = \omega^* - n_L P_L \tag{4.15}$$

which indirectly relates to the active power P and the reactive power Q, depending on θ.

This controller is called the RL controller. It has the same form as the droop controller designed for L inverter except that we need to obtain the transformed power P_L and Q_L based on θ.

After calculating the eigenvalues of T_L, we get $\lambda_{1,2} = \sin\theta \pm j\cos\theta$ that the real part $\sin\theta$ is positive when $\theta \in \left(0, \frac{\pi}{2}\right]$. According to the change of basis, the power transformation (4.11) just changed the coordinates, but the vector map did not change [37]. Hence, the mapping described by (4.10) indicates that P and Q have positive correlations with P_L and Q_L, respectively.

$$P \sim P_L \tag{4.16}$$

$$Q \sim Q_L \tag{4.17}$$

Then the relationship described in (4.12) and (4.13) can be passed onto P and Q as

$$P \sim P_L \sim \delta \tag{4.18}$$

$$Q \sim Q_L \sim E \tag{4.19}$$

which means, in the case of $\theta \in \left(0, \frac{\pi}{2}\right]$, the active power P has a positive correlation with the power angle δ, and the reactive power Q has a positive correlation with the voltage amplitude E.

Therefore, the RL controller can also take the form of

$$E = E^* - mQ \tag{4.20}$$

$$\omega = \omega^* - nP \tag{4.21}$$

which directly relates to the active power P and the reactive power Q, regardless of θ.

As a result, the effect of the impedance angle θ has been removed when $\theta \in \left(0, \frac{\pi}{2}\right]$.

4.2.2 RC Controller Analysis

Several works have been done as well in the case of R, C, and RC inverters [38] in order to research the parallel operation of inverters with different types of internal impedance.

In a similar fashion, the corresponding transformation matrix is the capacitive transformation matrix T_C

$$T_C = \begin{bmatrix} -\sin\theta & \cos\theta \\ -\cos\theta & -\sin\theta \end{bmatrix} \tag{4.22}$$

It transforms the matrix of generic power (4.1), (4.2) into the matrix of specific power when the impedance angle $\theta \in \left[-\frac{\pi}{2}, 0\right)$.

$$\begin{bmatrix} P_C \\ Q_C \end{bmatrix} = T_C \begin{bmatrix} P \\ Q \end{bmatrix} = \begin{bmatrix} -\dfrac{EV\sin\delta}{Z} \\ -\dfrac{EV\cos\delta - V^2}{Z} \end{bmatrix} \tag{4.23}$$

This power transformation (4.23) can also be written in the phasor diagram as

$$\begin{aligned} P_C + jQ_C &= \left(-P\sin\theta + Q\cos\theta\right) + j\left(-P\cos\theta - Q\sin\theta\right) \\ &= \left(-\sin\theta - j\cos\theta\right)\left(P + jQ\right) \\ &= \left(\cos\left(-\frac{\pi}{2} - \theta\right) + j\sin\left(-\frac{\pi}{2} - \theta\right)\right)\left(P + jQ\right) \\ &= e^{j\left(-\frac{\pi}{2} - \theta\right)}\left(P + jQ\right) \end{aligned} \tag{4.24}$$

In other words, the transformation matrix T_C rotates the power vector $P + jQ$ by $-\frac{\pi}{2} - \theta$ rad onto the axis aligned with the C inverter [21], as shown in Fig. 4.4.

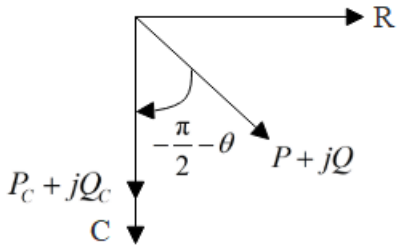

Fig. 4.4: Power transformation by matrix T_C.

This figure is originally from [21] but with modifications from the author.

Because the power angle δ is small enough, we obtain approximately

$$P_C \sim -\delta \tag{4.25}$$

$$Q_C \sim -E \tag{4.26}$$

then the droop controller takes the form of

$$E = E^* + m_C Q_C \tag{4.27}$$

$$\omega = \omega^* + n_C P_C \tag{4.28}$$

which indirectly relates to the active power P and the reactive power Q, depending on θ.

This controller is called the RC controller. It has the same form as the droop controller designed for C inverter in addition to needing to obtain the transformed power P_L and Q_L based on θ.

After calculating the eigenvalues for T_C, we get $\lambda_{1,2} = -\sin\theta \pm j\cos\theta$, which the real part $-\sin\theta$ is positive when $\theta \in \left[-\frac{\pi}{2}, 0\right)$. Similarly, according to the [37] and (4.23), we know that P and Q have positive correlations with P_C and Q_C, respectively.

$$P \sim P_C \tag{4.29}$$

$$Q \sim Q_C \tag{4.30}$$

Then the relationship described in (4.25) and (4.26) can be passed onto P and Q as

$$P \sim P_C \sim -\delta \tag{4.31}$$

$$Q \sim Q_C \sim -E \tag{4.32}$$

which means, when $\theta \in \left[-\frac{\pi}{2}, 0\right)$, the active power P has a negative correlation with the power angle δ, and the reactive power Q has a negative correlation with the voltage amplitude E.

Therefore, the RC controller can also take the form of

$$E = E^* + mQ \tag{4.33}$$

$$\omega = \omega^* + nP \tag{4.34}$$

which directly related to the active power P and the reactive power Q, regardless of θ.

As a consequence, the influence of the impedance angle θ has been removed when $\theta \in \left[-\frac{\pi}{2}, 0\right)$.

4.2.3 Universal Controller Analysis

Following the same idea described in the previous two subsections, the resistive transformation matrix T_R, also known as the universal transformation matrix T_U ,was proposed in [21].

$$T_U = \begin{bmatrix} \cos\theta & \sin\theta \\ -\sin\theta & \cos\theta \end{bmatrix} \tag{4.35}$$

It transforms the matrix of generic power (4.1), (4.2) into the matrix of specific power when the impedance angle $\theta \in \left(-\frac{\pi}{2}, \frac{\pi}{2}\right)$.

$$\begin{bmatrix} P_R \\ Q_R \end{bmatrix} = T_U \begin{bmatrix} P \\ Q \end{bmatrix} = \begin{bmatrix} \dfrac{EV\cos\delta - V^2}{Z} \\ -\dfrac{EV\sin\delta}{Z} \end{bmatrix} \tag{4.36}$$

which can also be written in the phasor diagram as

$$\begin{aligned} P_R + jQ_R &= \left(P\cos\theta + Q\sin\theta\right) + j\left(-P\sin\theta + Q\cos\theta\right) \\ &= \left(\cos(-\theta) + j\sin(-\theta)\right)\left(P + jQ\right) \\ &= e^{j(-\theta)}\left(P + jQ\right) \end{aligned} \tag{4.37}$$

The power transformation is drawn in Fig 4.5, and it can be expounded in the following. This transformation incorporates multi-scenarios into one case with a compact structure. The transformation matrix T_U rotates the power vector $P + jQ$ by $-\theta$ rad onto the axis aligned with the R inverter [21]. Specifically, clockwise if $\theta \in \left[0, \frac{\pi}{2}\right)$ and counterclockwise if $\theta \in \left(-\frac{\pi}{2}, 0\right]$.

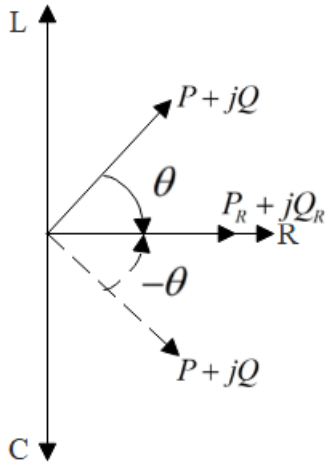

Fig. 4.5: Power transformation by matrix T_U.

This figure is originally from [21] but with modifications from the author.

Because the power angle δ is small enough in power systems, we have roughly

$$P_R \sim E \tag{4.38}$$

$$Q_R \sim -\delta \tag{4.39}$$

then the droop controller takes the form of

$$E = E^* - m_R P_R \tag{4.40}$$

$$\omega = \omega^* + n_R Q_R \tag{4.41}$$

which indirectly relates to the active power P and the reactive power Q, depending on θ.

This controller is called the R controller. It has the same form as the droop controller designed for R inverter except that we need to obtain the transformed power P_R and Q_R based on θ.

The eigenvalues of T_U are $\lambda_{1,2} = \cos\theta \pm j\sin\theta$ and its real part $\cos\theta$ is positive if $\theta \in \left(-\frac{\pi}{2}, \frac{\pi}{2}\right)$.

Similarly, the transitivity from P and Q to P_R and Q_R then to E and δ establishes the relationship

$$P \sim E \tag{4.42}$$

$$Q \sim -\delta \tag{4.43}$$

Therefore, UDC can also take the form of

$$E = E^* - mP \tag{4.44}$$

$$\omega = \omega^* + nQ \tag{4.45}$$

which directly related to the active power P and the reactive power Q, regardless of θ.

Naturally, the effect of the impedance angle θ has been removed when $\theta \in \left(-\frac{\pi}{2}, \frac{\pi}{2}\right)$.

It is obvious that the above relationship fails when the impedance is purely inductive, i.e., $\theta = \frac{\pi}{2}$, or capacitive, i.e., $\theta = -\frac{\pi}{2}$. However, there is always an equivalent series resistance (ESR) in series with the filter inductor in practice [21]. This is where the name of UDC comes from.

There are many ways to achieve the UDC principle so long as the relationship between the voltage and the power are consistent with that of the R inverter. RDC described in Chapter 3 is an attractive controller due to the improvements in power sharing and voltage regulation, and it will be regarded as UDC in this thesis for the rest of the contents.

In summary, UDC is applicable to the inverter that the internal impedance angle is in the range of $\left(-\frac{\pi}{2}, \frac{\pi}{2}\right)$ rad, i.e., all practical inverters, and it can be implemented by RDC.

4.3 Small-Signal Stability Analysis

4.3.1 Characteristic Equation

The mathematical descriptions of an inverter, i.e., (4.1) and (4.2), are used to derive the small-signal model [39], [40] of the inverter at the stable equilibrium operation point, i.e., E_e, δ_e, and V_e. Here, E_e is the RMS value of the source voltage magnitude, δ_e is the phase difference between the source voltage and the load voltage, and V_e is the RMS value of the load voltage magnitude. These parameters are the quiescent values when the system is in the steady state. It is assumed that any state variable is equal to the corresponding quiescent value plus the small variation, i.e., $x = x_e + \Delta x$. For example, $E = E_e + \Delta E$.

Note that there is no variation for load voltage because the load voltage is usually a constant value with insignificant changes in power systems.

Linearizing (4.1) around the equilibrium point, we have

$$\begin{aligned} P_e + \Delta P &= \frac{\cos\theta}{Z}\left[\left(E_e + \Delta E\right)V_e \cos\left(\delta_e + \Delta\delta\right) - V_e^{\,2}\right] + \frac{\sin\theta}{Z}\left(E_e + \Delta E\right)V_e \sin\left(\delta_e + \Delta\delta\right) \\ &= \frac{\cos\theta}{Z}\left[\left(E_e + \Delta E\right)V_e\left(\cos\delta_e\cos\Delta\delta - \sin\delta_e\sin\Delta\delta\right) - V_e^{\,2}\right] \\ &\quad + \frac{\sin\theta}{Z}\left(E_e + \Delta E\right)V_e\left(\sin\delta_e\cos\Delta\delta + \cos\delta_e\sin\Delta\delta\right) \end{aligned} \tag{4.40}$$

Because $\Delta\delta$ is small enough, $\sin\Delta\delta \cong \Delta\delta$, $\cos\Delta\delta \cong 1$. Then above equation becomes

$$\begin{aligned} P_e + \Delta P &= \frac{\cos\theta}{Z}\left[\left(E_e + \Delta E\right)V_e\left(\cos\delta_e - \Delta\delta\sin\delta_e\right) - V_e^{\,2}\right] \\ &\quad + \frac{\sin\theta}{Z}\left(E_e + \Delta E\right)V_e\left(\sin\delta + \Delta\delta\cos\delta_e\right) \\ &= \frac{\cos\theta}{Z}\left(E_eV_e\cos\delta_e - E_eV_e\Delta\delta\sin\delta_e + \Delta EV_e\cos\delta_e - \Delta EV_e\Delta\delta\sin\delta_e - V_e^{\,2}\right) \\ &\quad + \frac{\sin\theta}{Z}\left(E_eV_e\sin\delta_e + E_eV_e\Delta\delta\cos\delta_e + \Delta EV_e\sin\delta_e + \Delta EV_e\Delta\delta\cos\delta_e\right) \end{aligned} \tag{4.41}$$

Since the product of two small variations is negligible, then above equation further turns into

$$\begin{aligned} P_e + \Delta P &= \frac{\cos\theta}{Z}\left(E_eV_e\cos\delta_e - EV_e\Delta\delta\sin\delta_e + \Delta EV_e\cos\delta_e - V_e^{\,2}\right) \\ &\quad + \frac{\sin\theta}{Z}\left(E_eV_e\sin\delta_e + E_eV_e\Delta\delta\cos\delta_e + \Delta EV_e\sin\delta_e\right) \\ &= \frac{\cos\theta}{Z}\left(E_eV_e - V_e^{\,2}\right) + \frac{\sin\theta}{Z}E_eV_e\sin\delta_e \\ &\quad + \frac{V_e}{Z}\left(\cos\delta_e\cos\theta + \sin\delta_e\sin\theta\right)\Delta E + \frac{E_eV_e}{Z}\left(-\sin\delta_e\cos\theta + \cos\delta_e\sin\theta\right)\Delta\delta \end{aligned} \tag{4.42}$$

Then, we obtain

$$\Delta P(s) = \frac{V_e}{Z}\left(\cos\delta_e\cos\theta + \sin\delta_e\sin\theta\right)\Delta E(s) + \frac{E_e V_e}{Z}\left(-\sin\delta_e\cos\theta + \cos\delta_e\sin\theta\right)\Delta\delta(s) \quad (4.43)$$

Similarly, we can linearize the reactive power and the controller Equations.

$$\Delta Q(s) = \frac{V_e}{Z}\left(\cos\delta_e\sin\theta - \sin\delta_e\cos\theta\right)\Delta E(s) - \frac{E_e V_e}{Z}\left(\sin\delta_e\sin\theta + \cos\delta_e\cos\theta\right)\Delta\delta(s) \quad (4.44)$$

$$s\Delta E(s) = -m\Delta P(s) \quad (4.45)$$

$$\Delta\omega(s) = n\Delta Q(s) \quad (4.46)$$

Moreover, there is a relationship between the variation of frequency and the variation of angle

$$\Delta\omega(s) = s\Delta\delta(s) \quad (4.47)$$

Normally, the active power and the reactive power are measured by using a low pass filter [20]

$$\frac{\omega_f}{s+\omega_f} \quad (4.48)$$

Substituting (4.43) and (4.44) into the right item of equations (4.45) and (4.46), and taking (4.47) and (4.48) into consideration, we have

$$s\Delta E(s) = \frac{-m\omega_f}{s+\omega_f}\times \left[\frac{V_e}{Z}\left(\cos\delta_e\cos\theta + \sin\delta_e\sin\theta\right)\Delta E(s) + \frac{E_e V_e}{Z}\left(-\sin\delta_e\cos\theta + \cos\delta_e\sin\theta\right)\Delta\delta(s)\right] \quad (4.49)$$

$$s\Delta\delta(s) = \frac{n\omega_f}{s+\omega_f}\times \left[\frac{V_e}{Z}\left(\cos\delta_e\sin\theta - \sin\delta_e\cos\theta\right)\Delta E(s) - \frac{E_e V_e}{Z}\left(\sin\delta_e\sin\theta + \cos\delta_e\cos\theta\right)\Delta\delta(s)\right] \quad (4.50)$$

Then we can obtain the small-signal model of the closed-loop system of an inverter in terms of $\Delta\delta$ by substituting (4.49) into (4.50).

$$as^4\Delta\delta(s) + bs^3\Delta\delta(s) + cs^2\Delta\delta(s) + ds^1\Delta\delta(s) + es^0\Delta\delta(s) = 0 \quad (4.51)$$

where

$$\begin{aligned} a &= Z^2 \\ b &= 2\omega_f Z^2 \\ c &= \omega_f^2 Z^2 + \left(\cos\delta_e\cos\theta + \sin\delta_e\sin\theta\right)\left(m + nE\right)\omega_f VZ \\ d &= \left(\cos\delta_e\cos\theta + \sin\delta_e\sin\theta\right)\left(m + nE\right)\omega_f^2 VZ \\ e &= mn\omega_f^2 EV^2 \end{aligned} \quad (4.52)$$

The characteristic equation of above small-signal model is

$$as^4 + bs^3 + cs^2 + ds + e = 0 \quad (4.53)$$

4.3.2 Root Locus

Using the parameters provided by [21], which are summarized in Table 4.2, we can investigate the system stability with the help of root locus.

Parameter	Value	Unit
V_{DC}	30	V
f	50	Hz
f_s	10	kHz
E^*	12	V
ω^*	100π	rad/s
ω_f	10	rad/s
L	7	mH
R_p	1	Ω
C	1	μF
K_e	20	
m	0.48	
n	0.03	

Table 4.2: Stability parameters of an inverter equipped with UDC.

These data are originally from [21].

The root locus is a general method that can be used to plot the roots of any polynomial with respect to any one real parameter that enters the equation linearly [41]. However, there are two non-linear items, i.e., *c* and *d*, in the characteristic equation (4.53). Therefore, we cannot get the root locus directly by using MATLAB function rlocus, but we can obtain it indirectly by calculating each root and then combining them to draw a plot. Then, the resulting root locus plot in terms of impedance angle is shown in Fig. 4.6.

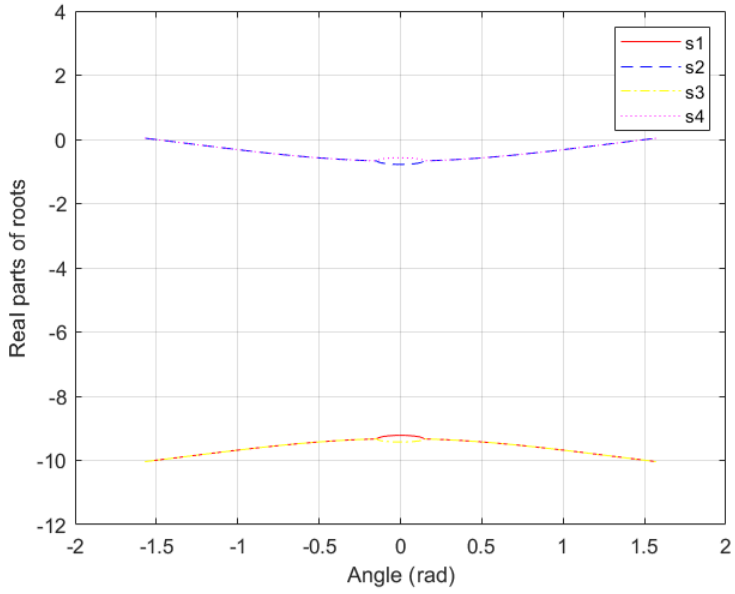

Fig. 4.6: Real parts of roots of an inverter equipped with UDC.

4.3.3 Routh's Criterion

There are many ways to determine the stability of control system. In this subsection, Routh's criterion was used to research the stability of an inverter equipped with UDC. The Routh array is

s^4	a	c	e
s^3	b	d	
s^2	$\frac{bc-ad}{b}$	$\frac{be}{d}$	
s^1	$d-\frac{b^3e}{d(bc-ad)}$		
s^0	e		

Table 4.3: Routh array of an inverter equipped with UDC.

A system is stable only if all the elements in the first column of Routh array are positive [41]. Since a, b, e are all greater than zero, attention should be focused on the third and fourth coefficients of Routh array. After defining $A=\frac{bc-ad}{b}$ and $B=d-\frac{b^3e}{d(bc-ad)}$ as the third and fourth coefficients, we obtained the corresponding values over the range of $\left[-\frac{\pi}{2},\frac{\pi}{2}\right]$.

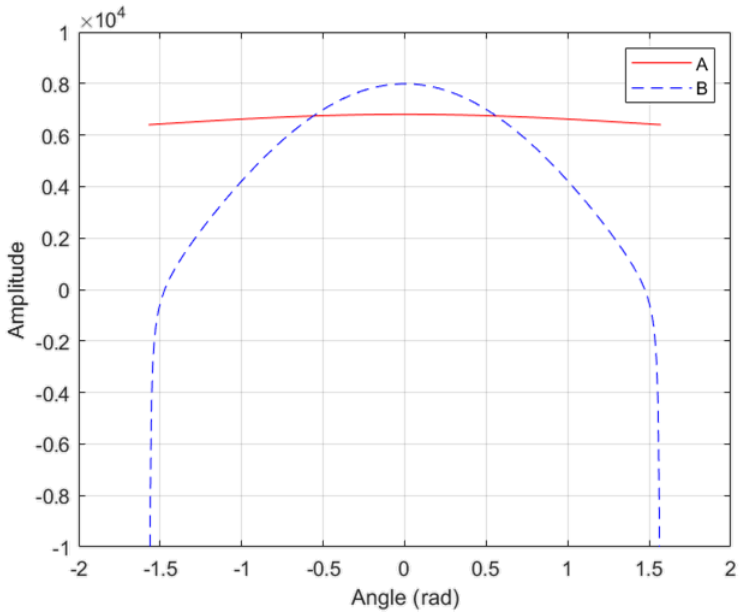

Fig. 4.7: Routh coefficients of an inverter equipped with UDC.

In Fig. 4.6, when the impedance angle in the range of $\left[-\frac{\pi}{2},\frac{\pi}{2}\right]$, the real parts of all four roots are negative, which means all the poles of the systems are located at the left-hand *s*-plan (LHP), except for a narrow range of two sides near the boundaries.

In Fig. 4.7, both A and B are positive if the impedance angle in the range of $\left[-\frac{\pi}{2},\frac{\pi}{2}\right]$ except for a narrow range of two sides near the boundaries.

Taking ESR into consideration, it is reasonable to conclude that the system of an inverter equipped with UDC is stable under the condition of Table 4.2.

The MATLAB codes for small-signal model stability are attached in Appendix B. The precise explanations of concepts and applications of control theory can refer to [41]. More detailed reasoning discussions, simulation results, and experimental results of UDC can refer to [21].

Chapter 5

Self-Synchronized Universal Droop Controller

At present, a grid-connected inverter is usually controlled as a voltage supply due to the superiorities, such as taking part in voltage regulation, which is non-existent if the inverter is controlled as a current supply. The typical control structure is shown in Fig. 5.1. It consists of four loops in such a way from outside to inside: a synchronization unit to synchronize the inverter output voltage with the grid voltage, a power loop to control the power exchanged with the grid, and a voltage and a current loop to regulate the output voltage and current, respectively.

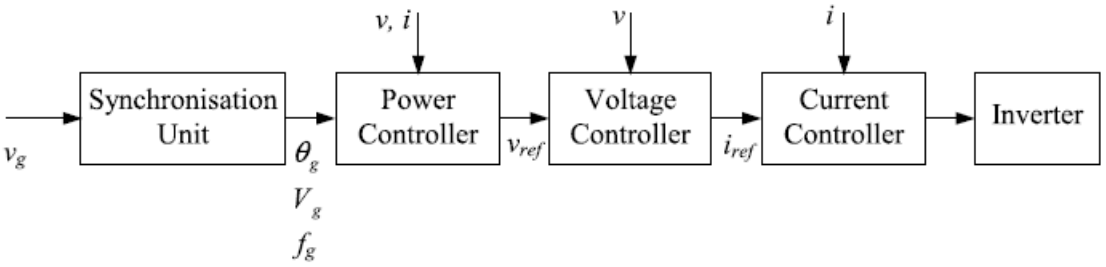

Fig. 5.1: Control structure of grid-connected inverter [19].

Among the above control objectives, the synchronization is always given the highest priority. In order to get synchronization, a PLL is usually placed in the outermost loop of the controller. The synchronization unit is often required to provide the amplitude and the frequency, in addition to the phase, of the fundamental component of the grid voltage [19]. However, there are several inevitably negative impacts in this kind of control system due to the existence of PLL, such as the characteristic of non-linearity, concomitantly complicating the system and the potential competition under the condition of multi-PLL operation. Therefore, it would be better if we can incorporate the synchronization mechanism into the controller. SUDC [23] was proposed in such condition to meet the demand that removes the required synchronization unit.

5.1 Relationship Deduction

5.1.1 Phase-Locked Loop

A PLL is a circuit synchronizing an output signal with an input signal in frequency as well as in phase [42]. The PLL consists of three basic functional blocks: a phase detection (PD), a loop filter (LF), and a voltage-controlled oscillator (VCO). Its block diagram is shown in Fig. 5.2.

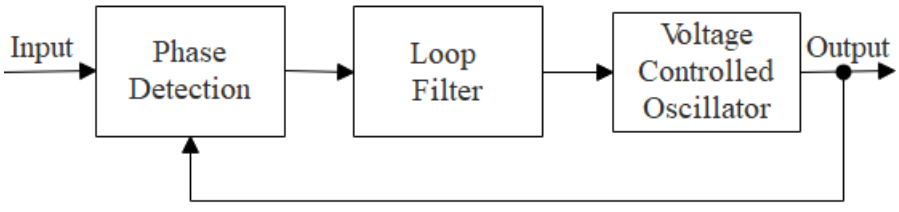

Fig. 5.2: Block diagram of PLL operational mechanism.

This figure is originally from [5] but with modifications from the author.

Its operating principle is illustrated in the following. The PD compares the phase difference (error) between the input signal and the output signal as output and then passes it to the LF for extracting the DC component. The DC component is amplified and then passed to the VCO, which could be a PI controller to generate the frequency of the output signal [5]. The generated frequency is integrated to form the phase of the output signal. If the frequency of the output signal is locked with the frequency of the input signal, then the error between the input signal and the output signal is driven to zero eventually by the feedback control mechanism. Consequently, the phase of the output signal is locked with the phase of the input signal. Therefore, this is the reason why it is called the PLL.

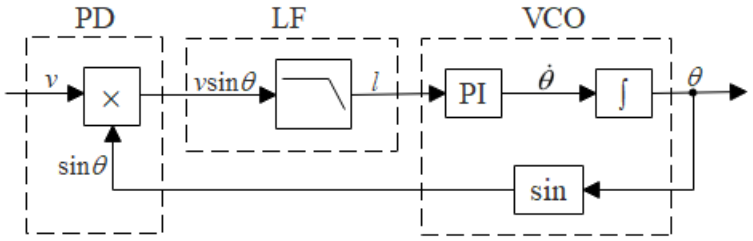

Fig. 5.3: Block diagram of a basic PLL.

This figure is originally from [5] but with modifications from the author.

Fig. 5.3 is a simple implementation of PLL in power systems. The PD is a multiplier, the LF is a low-pass filter (LPF), and the VCO, which consists of a PI controller, an integrator, and a sinusoidal function [5]. Assumed that the input signal is $v = \mathrm{V}\cos\theta_0$ with phase $\theta_0 = \omega_0 t + \delta_0$ and the output signal is the phase $\theta = \omega t + \delta$. Then the output of the PD is

$$\begin{aligned} v\sin\theta &= \mathrm{V}\sin\theta\cos\theta_0 \\ &= \frac{\mathrm{V}}{2}\sin(\theta-\theta_0) + \frac{\mathrm{V}}{2}\sin(\theta+\theta_0) \\ &= \frac{\mathrm{V}}{2}\sin[(\omega-\omega_0)t + (\delta-\delta_0)] + \frac{\mathrm{V}}{2}\sin[(\omega+\omega_0)t + (\delta+\delta_0)] \end{aligned} \tag{5.1}$$

Due to the algebraic relation inside the above function, the first term is a low-frequency component that includes the phase difference between *v* and *θ*; the second one is a high-frequency counterpart, which is out of our interest and should be removed through an LPF. Hence, the output of the LPF is

$$l = \frac{\mathrm{V}}{2}\sin[(\omega-\omega_0)t + (\delta-\delta_0)] \tag{5.2}$$

which is fed into a PI controller to generate the estimated frequency ω until $l = 0$ [5]. Then the estimated frequency $\dot{\theta}$ is integrated to produce the output signal θ. The output signal θ is combined with the sine function and fed back to the PD to establish the feedback loop. When the system is in steady state, *l* is driven to zero and $\theta = \theta_0$, indicating that the phase of the output signal θ is locked with the phase of the input signal v.

Based on the above analysis, this kind of PLL can provide the phase and frequency information, but it cannot provide the information of the voltage amplitude. In order to obtain the amplitude information of voltage, an enhanced PLL (EPLL) and its application were proposed in [43], [44].

A set of differential Equations for designing EPLL is summarized by [22].

$$\begin{cases} \dot{E} = \mu_1 d \sin\theta \\ \dot{\omega} = \mu_2 dE \cos\theta \\ \dot{\theta} = \mu_3 \dot{\omega} + \omega \end{cases} \tag{5.3}$$

where d is the error between the input signal v and the output signal e. μ is the diagonal matrix chosen for minimizing the cost function.

In that event, the block diagram of EPLL is constructed in such a way shown in Figure 5.4. More detailed discussion can refer to [22], [43], [44].

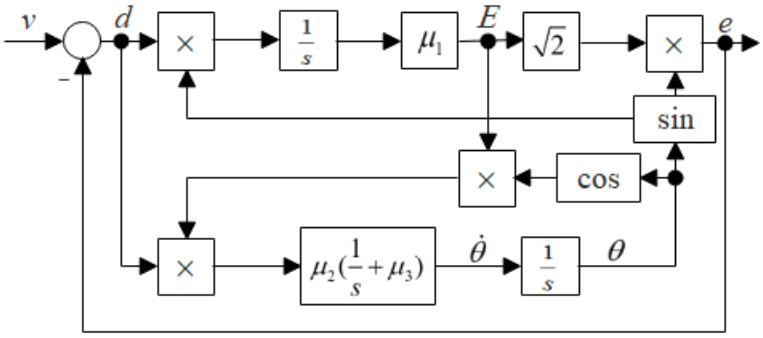

Fig. 5.4: Block diagram of EPLL.

This figure is originally from [22] but with modifications from the author.

Compared to the basic PLL, the EPLL has one more channel, the amplitude channel, to estimate the amplitude of the input signal, in addition to the frequency channel to estimate the frequency and the phase of the input signal.

In summary, more advanced PLLs are emerging today to improve the performance and add some new functionality, such as the EPLL discussed above. Although PLL can achieve the functionality of the synchronization, the concomitant shortcomings are evident. The character caused by highly non-linear nature [5] will lead to complicating the systems [45] or even destroy the stability [46]. Furthermore, tuning parameters of PLLs is usually tricky and time-consuming, and it is worse if there are multiple PLLs in a system due to the competition.

5.1.2 Structural Resemblance

The block diagram of CDC for an inverter with resistive impedance is redrawn in Fig. 5.5.

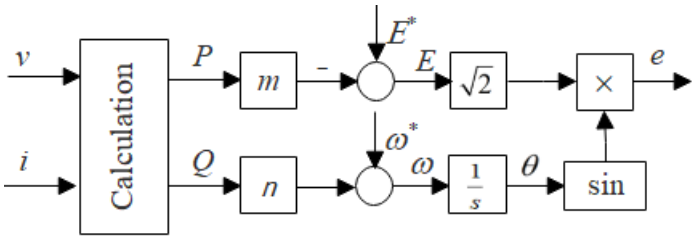

Fig. 5.5: Block diagram of CDC without the integral effect.

This figure is based on a similar figure from [22].

The mathematical expressions of the above controller are

$$E = E^* - mP \tag{5.4}$$

$$\omega = \omega^* + nQ \tag{5.5}$$

As we have already known from Chapter 3, the RMS value of voltage E can be dynamically realized by integrating

$$\Delta E = E^* - E - mP \tag{5.6}$$

until $\Delta E = 0$ instead of statically setting $E = E^* - mP$.

Similarly, we can apply this method to the frequency loop. Then the frequency ω can be achieved by integrating

$$\Delta\omega = \omega^* - \omega + nQ \tag{5.7}$$

until $\Delta\omega$=0 instead of statically setting $\omega = \omega^* + nQ$.

Then the block diagram of CDC with such integral effects is drawn in Fig. 5.6.

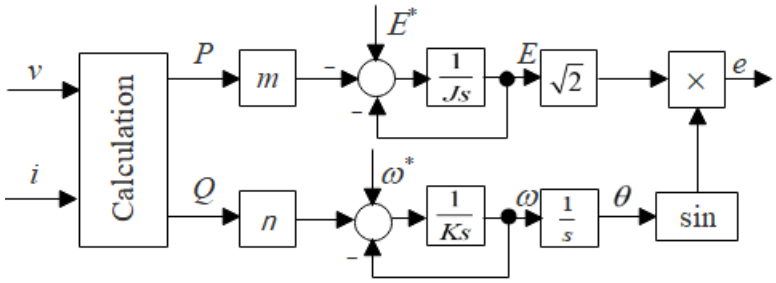

Fig. 5.6: Block diagram of CDC with the integral effect.

This figure is based on a similar figure from [22].

In Fig. 5.6, there are two integral time constants, i.e., *J* and *K*, in the voltage and frequency loops. This integral effect is equivalent to adding a low-pass filter $\frac{1}{Js+1}$ to the voltage loop, and a low-pass filter $\frac{1}{Ks+1}$ to the frequency loop of the conventional droop controller.

For example, the transfer function of the added item for the voltage loop is

$$J(s)=\frac{\frac{1}{Js}}{1+\frac{1}{Js}}=\frac{1}{Js+1} \tag{5.8}$$

When the system is in the steady state, the inputs to the integrators should be zero, which turn (5.6) and (5.7) into (5.4) and (5.5), respectively. Consequently, these two controllers are identical in the steady state.

The current i flowing through the impedance $Z=R$ is

$$i=\frac{e-v}{R}=-\frac{v-e}{R} \tag{5.9}$$

This relationship can be used to close the loop between source voltage *e* and terminal voltage *v*.

Note that $i=0$ indicates $e=v$, which means e is synchronized with v.

The active power *P* and the reactive power *Q* are usually calculated utilizing the output voltage v and the output current i. However, the authors in [22] pointed out that it would be better if we use the source voltage e instead of the terminal voltage v to calculate power because e is available internally. Note that it does ignore the power losses of the filter inductor, but the influence is negligible. By doing so, it converts the power delivered to the load to the power generated by the supply. Then the active power and the reactive power of an inverter can be calculated according to the instantaneous power theory [47].

The active power is calculated by

$$P=\frac{1}{T}\int_{t-T}^{t}(e\cdot i)\,\mathrm{d}t \tag{5.10}$$

where *T* is the period of the system.

After applying the Laplace transform, it is equivalent to passing the instantaneous active power $p=e\cdot i$ through the hold filter $H(s)=\frac{1-e^{-Ts}}{Ts}$ to obtain the average active power *P* [22].

The reactive power can be obtained similarly.

A voltage [22] was defined as

$$e_q = \sqrt{2}E\sin(\theta - \frac{\pi}{2}) = -\sqrt{2}E\cos\theta \tag{5.11}$$

which has the same amplitude $\sqrt{2}E$ with e but has delayed the phase angle by $\frac{\pi}{2}$ rad.

Then, the reactive power is calculated by

$$Q = \frac{1}{T}\int_{t-T}^{t} e_q i \mathrm{d}t \tag{5.12}$$

A calculation example is given as follows.

Suppose $i = \sqrt{2}I\sin\delta$, then

$$\begin{aligned} Q &= \frac{1}{T}\int_{t-T}^{t} e_q i \mathrm{d}t \\ &= \frac{1}{T}\int_{t-T}^{t} 2EI\sin(\theta - \frac{\pi}{2})\sin\delta \mathrm{d}t \\ &= \frac{EI}{T}\int_{t-T}^{t} [\cos(\theta - \delta - \frac{\pi}{2}) - \cos(\theta + \delta - \frac{\pi}{2})]\mathrm{d}t \\ &= \frac{EI}{T}\int_{t-T}^{t} [\sin(\theta - \delta) - \sin(\theta + \delta)]\mathrm{d}t \\ &= EI\sin(\theta - \delta) \end{aligned} \tag{5.13}$$

which is indeed the reactive power generated by e and i [22].

To send the desired power to the load for an inverter in the set mode of grid-connected scenarios, the voltage reference E^* is set as the grid voltage E, and the frequency reference ω^* is set as the grid frequency ω. Then, the block diagram of CDC becomes

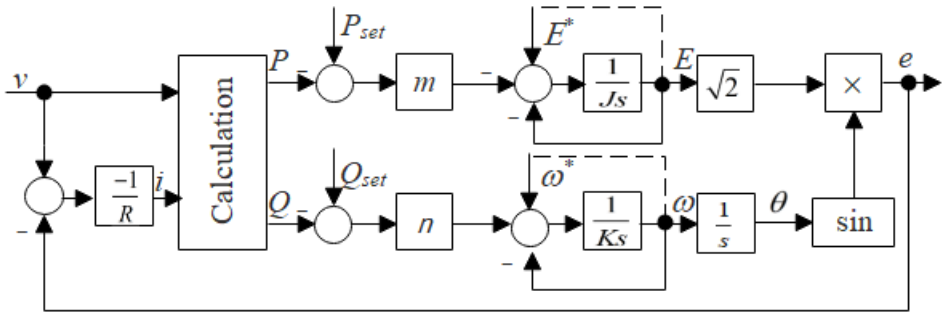

Fig. 5.7: Block diagram of CDC with the integral effect and the resistive impedance.

This figure is based on a similar figure from [22].

When the system is in the steady state, $e = v$. Under the circumstance, the loops around the integrators are canceled out, and the block diagram of CDC further becomes Fig. 5.8 after taking (5.10) and (5.12) into consideration.

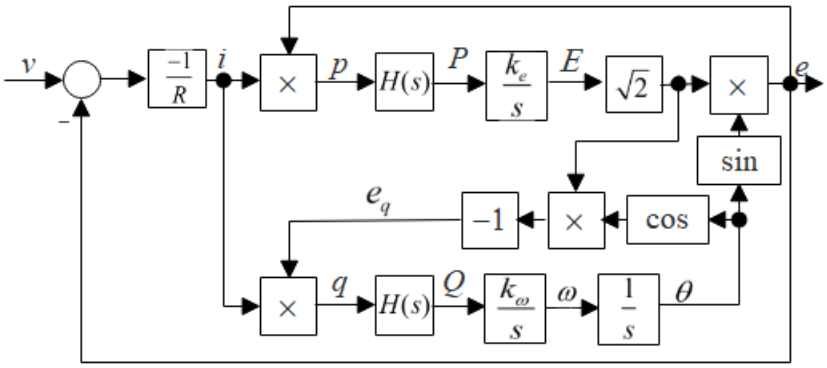

Fig. 5.8: Block diagram of CDC in the form of PLL.

This figure is based on a similar figure from [22].

The proportional coefficients are lumped in a way that $k_e = \frac{-m}{J}$ and $k_\omega = \frac{n}{K}$.

Comparing Fig 5.4 with Fig 5.8, CDC structurally resembles the EPLL. More specifically, if $R = -\sqrt{2}E$, $\mu_1 = k_e$, $\mu_2 = k_\omega$, $\mu_3 = 0$, and two hold filters $H(s)$ are removed, these two block diagrams are very similar to each other. In other words, CDC is the EPLL under the above conditions. The controller can operate as a synchronization unit when there is no power exchange; the controller can also operate as a droop controller when there is power exchange.

In summary, the droop controller structurally resembles the EPLL. Therefore, the dedicated synchronization unit, which generally is PLL, can be removed in theory.

5.2 Mechanism Analysis

Based on the original UDC, five adjustments are made to form the SUDC in order to realize the comprehensive functionality. The block diagram of SUDC is shown in Fig. 5.9.

(1) In order to achieve the synchronization, the virtual current i_v comes into being to generate the calculation current before the inverter is connected to the grid when the grid current i_g is unavailable. It can be done by passing the voltage error $v - v_g$ through a virtual impedance $Ls + R$.

(2) In order to switch current after finishing the synchronization and connecting the inverter to the power grid, a switch S_i is added so that i_g is used to calculate power when i_g is available.

(3) In order to extend the operation mode of UDC to the grid-connected scenarios, especially for the set sub-mode, two summation blocks are added after the power calculation block to compare the measured power P and Q with the power reference P_{set} and Q_{set}. In the steady state, i.e., $V = E^*$ and $\omega = \omega^*$, $P = P_{set}$ and $Q = Q_{set}$.

(4) In order to switch the operation modes of the inverter for active power, a switch S_P is added to enable or disable the addition of the term $k_e(E^* - V)$.

(5) In order to obtain the zero-error tracking of reactive power, i.e., $Q = Q_{set}$, an integrator $\frac{k_\omega}{s}$ is added along with the reset function by turning switch S_Q on to take effect or off for no effect.

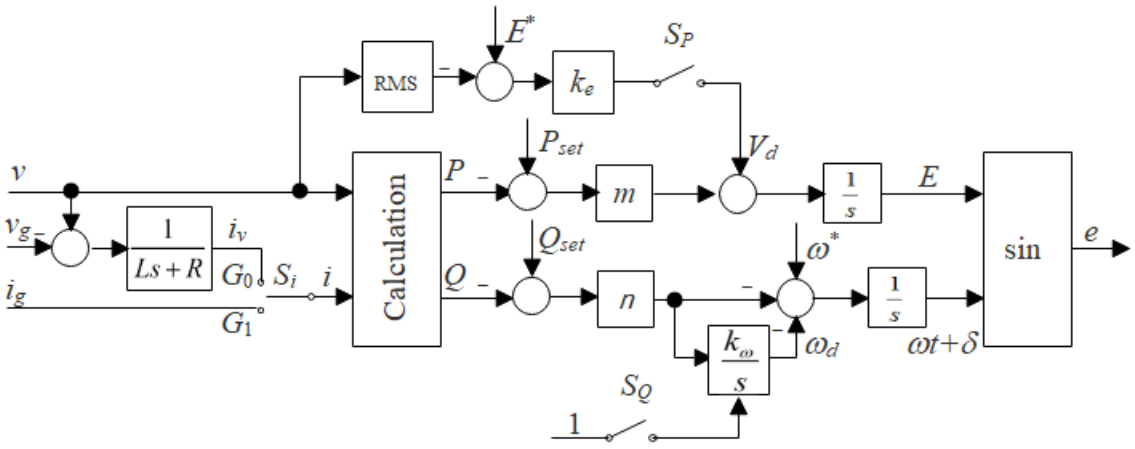

Fig. 5.9: Block diagram of SUDC.

This figure is originally from [23] but with modifications from the author.

The positions and influences of switches in SUDC are summarized in Table 5.1.

Switch	Position	Function
S_i	G_0	Prepare for synchronization; bring i_v into the calculation block
	G_1	Operate in the set/droop mode; bring i_g into the calculation block
S_P	ON	Operate in the droop mode; enable the addition of $k_e(E^*-V)$
	OFF	Operate in the set mode; disable the addition of $k_e(E^*-V)$
S_Q	ON	Operate in the droop mode; enable the reset function of $\frac{k_\omega}{s}$
	OFF	Operate in the set mode; disable the reset function of $\frac{k_\omega}{s}$

Table 5.1: Positions and functions of three switches in SUDC.

From Fig. 5.8, the controller can be presented by

$$\dot{E} = V_d + m(P_{set} - P) \tag{5.14}$$

$$\omega = \omega^* + \omega_d - n(Q_{set} - Q) \tag{5.15}$$

with

$$V_d = \begin{cases} k_e(E^* - V_o), (S_P = \text{ON}) \\ 0, (S_P = \text{OFF}) \end{cases}$$

$$\omega_d = \begin{cases} 0, (S_Q = \text{ON}) \\ \frac{nk_\omega}{s}(Q - Q_{set}), (S_Q = \text{OFF}) \end{cases}$$

where k_ω is a positive proportional gain, called the frequency coefficient.

The virtual current is

$$i_v = \frac{v - v_g}{Ls + R} \tag{5.16}$$

where parameters *L* and *R* can be chosen smaller than the inductance and resistance of the filter inductor to expedite the synchronization. Moreover, to filter out the effect of the harmonics, the ratio of $\frac{L}{R}$ can be chosen larger than the fundamental frequency of the power grid [23].

The active power P and the reactive power Q are calculated from the output voltage v and current i, which can be switched between the virtual current i_v and the grid current i_g. A low-pass filter or a hold filter should be adopted to filter out the ripples of power so that *P* and *Q* only contain the DC components [22].

5.2.1 Self-Synchronization Mode

The first step for an inverter being operated in the grid-connected mode is to synchronize its output voltage v with the grid voltage v_g.

When S_i is at G_0 and both S_P and S_Q are OFF, the inverter is operated in the self-synchronization mode. When the system is in the steady state, the active power P and the reactive power Q are controlled around their set-points P_{set} and Q_{set}, respectively. More specifically, both references are set as zero in such mode. However, both P and Q are equal to zero before the inverter is connected to the grid due to the disconnection. In order to realize the synchronization, a virtual impedance is introduced to generate a virtual current according to the voltage difference $v - v_g$. In doing so, the controller can be presented by

$$\dot{E} = m(P_{set} - P) \tag{5.17}$$

$$\omega = \omega^* + \frac{nk_\omega}{s}(Q - Q_{set}) - n(Q_{set} - Q) \tag{5.18}$$

Since P_{set} and Q_{set} are both set as zero, in the steady state, regulating the virtual current to be zero results in $v = v_g$, which means that the output voltage v of the inverter synchronize with the grid voltage v_g.

After achieving the synchronization, the circuit breaker interfaced between the inverter and the grid can be turned on to connect the inverter to the grid. After finishing the connection, the switch S_i should be turned to G_1 so that the grid current i_g can be used for power calculation.

5.2.2 Set Mode

After the inverter is synchronized with and connected to the grid, the inverter can operate in the set mode for the active power and the reactive power simultaneously or separately.

When S_i is at G_1 and S_P is turned off, there is

$$\dot{E} = m(P_{set} - P) \tag{5.19}$$

When the system is in the steady state, the voltage settles down at a constant value, resulting in

$$P = P_{set} \tag{5.20}$$

Therefore, the desired active power P_{set} is sent to the grid from the inverter.

When S_i is at G_1 and S_Q is turned off, there is

$$\omega = \omega^* + \frac{nk_\omega}{s}(Q - Q_{set}) - n(Q_{set} - Q) \tag{5.21}$$

When the system is in the steady state, the frequency settles down at a certain value, resulting in

$$Q = Q_{set} \tag{5.22}$$

Therefore, the desired reactive power Q_{set} is sent to the grid from the inverter.

5.2.3 Droop Mode

After the inverter is synchronized with and connected to the grid, the inverter can also operate in the droop mode for the active power and the reactive power simultaneously or separately.

When S_i is at G_1 and S_P is turned on, there is

$$\dot{E} = k_e(E^* - V_o) + m(P_{set} - P) \tag{5.23}$$

When the system is in the steady state, the voltage settles down at a constant value, resulting in

$$P = P_{set} + \frac{k_e}{m}(E^* - V_o) \tag{5.24}$$

Therefore, the droop function of the active power with respect to the voltage takes effect. The active power sent to the grid is automatically regulated according the grid voltage V.

When S_i is at G_1 and S_Q is turned on, there is

$$\omega = \omega^* - n(Q_{set} - Q) \tag{5.25}$$

When the system is in the steady state, the voltage settles down at a constant value, resulting in

$$Q = Q_{set} + \frac{\omega - \omega^*}{m} \tag{5.26}$$

Therefore, the droop function of the reactive power with respect to the frequency function. The reactive power sent to the grid is automatically regulated according the grid frequency ω.

In summary, there are four combinations of the modes with respect to the set mode and the droop mode for powers, and the operation modes of the inverter in the grid-connected scenarios are listed in Table 5.2.

Operation mode	Switch S_i	Switch S_P	Switch S_Q
Self-synchronization mode	G_0	OFF	OFF
P_S mode, Q_S mode	G_1	OFF	OFF
P_S mode, Q_D mode	G_1	OFF	ON
P_D mode, Q_S mode	G_1	ON	OFF
P_D mode, Q_D mode	G_1	ON	ON

Table 5.2: Operation modes of an inverter equipped with SUDC.

This table is originally from [23] but with modifications from the author.

5.3 Simulation

Simulations were carried out to verify the self-synchronization mode of the inverter equipped with SUDC described in the previous subsection.

5.3.1 Preparations and Set-ups

When the inverter equipped with SUDC is under self-synchronization configuration, Fig. 5.9 becomes Fig. 5.10.

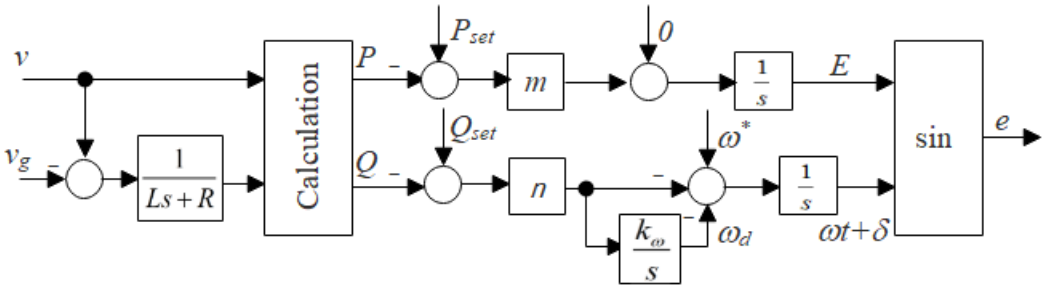

Fig. 5.10: Block diagram of SUDC in the self-synchronization mode.

To put the simulation in a way suitable for studying the self-synchronized operational mechanism, an inverter was replaced with a controlled voltage source with an internal impedance for simplicity. To emulate the real residential standard voltage in United States, 240 V of RMS value was set as the grid voltage RMS value, with voltage frequency 60 Hz.

The time of achieving synchronization varies as the starting time changes. Two typical circumstances were conducted in MABLAB/Simulink, i.e., the initial phases of grid voltage are 0° and 90°.

The simulation parameters are listed in Table 5.3.

Description	Parameter	Value	Unit
Grid voltage RMS value	V_g	240	V
Grid frequency	f	60	Hz
Internal resistance	R_I	1	Ω
Internal inductance	L_I	1	mH
Load resistance	R	1	MΩ
Virtual resistance	R	500	Ω
Virtual inductance	L	25	H
Voltage drop coefficient	m	60	
Frequency boost coefficient	n	60	
Frequency coefficient	k_ω	0.1	

Table 5.3: Simulation parameters for verifying self-synchronization mechanism.

5.3.2 Results and Analysis

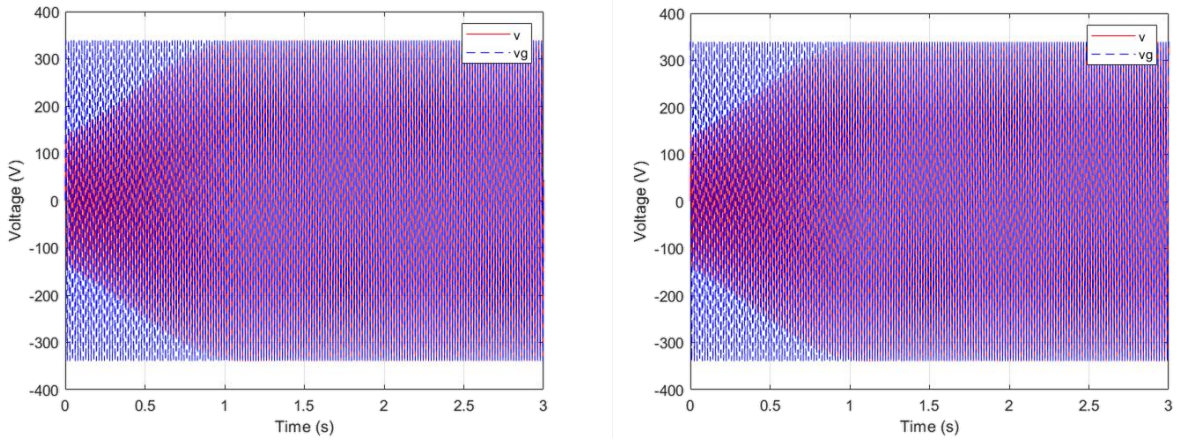

(a) Output voltage and grid voltage;

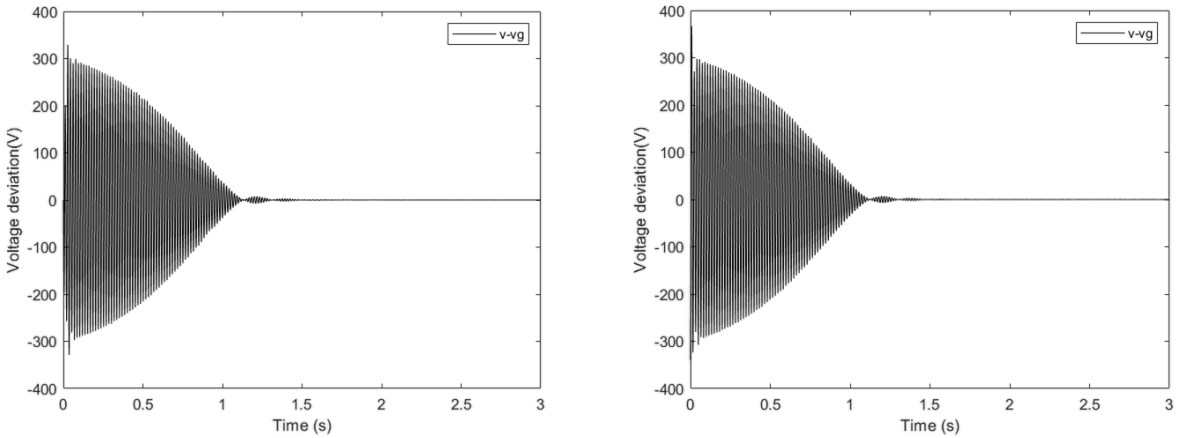

(b) Voltage deviation;

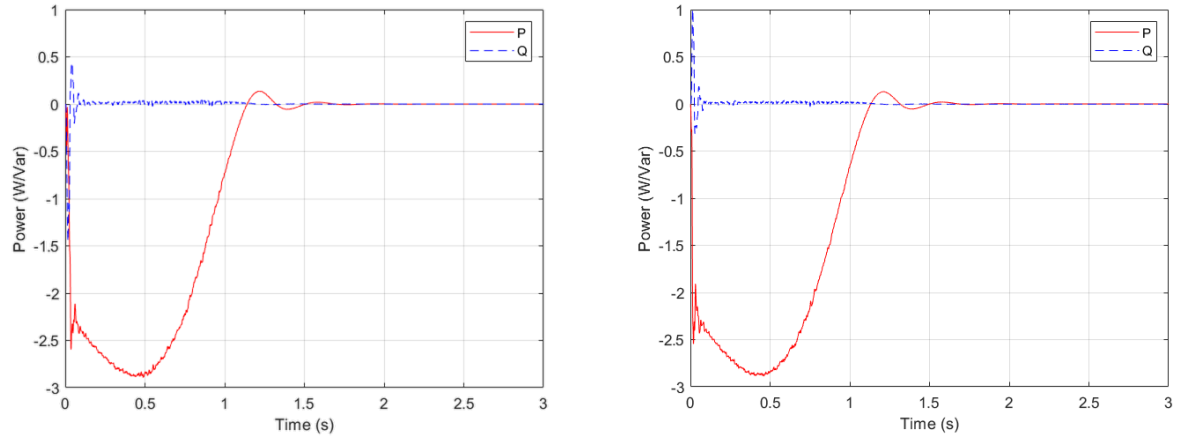

(c) Active power and reactive power;

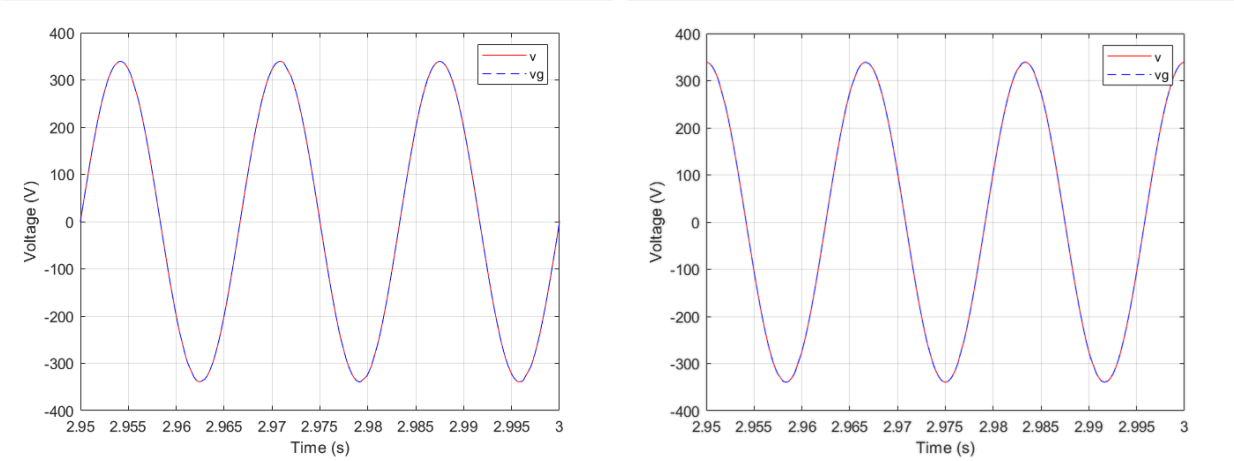

(d) Steady-state voltage.

Fig. 5.11: Simulation results.

In Fig. 5.11, the left column shows the results when the initial phase of grid voltage is 0°, the right column shows the results when the initial phase of grid voltage is 90°. After an approximate response of 1.5 s, the output voltage was synchronized with the grid voltage, and the steady-state voltage in Fig. 5.11 (d) indicates the frequency is 60 Hz. Thus, the self-synchronization mechanism was approved.

The simulation block diagrams are attached in Appendix C. The future works of this chapter are to further verify the set mode and drop mode when the inverter equipped with SUDC is operated in the grid-connected mode, and to realize the integrated functionality of SUDC.

In summary, an inverter equipped with SUDC can realize synchronization with the grid before the connection, without the must-have dedicated synchronization unit. An inverter equipped with SUDC can not only operate in the set mode to send the desired power to the grid, but can also maintain the droop characteristics for accurate proportional power sharing and tight load voltage regulation the same as the inverter equipped with UDC according to the simulation and experimental results from [23].

Chapter 6

Conclusions

The inverter has a pivotal role in AC microgrid integration. A microgrid can operate either in the stand-alone mode or in the grid-connected mode, as does an inverter. There are two main issues regarding the use of CDC in stand-alone mode. The first one is how to share the power of inverters in proportion to their power rating; the second one is how to reduce the load voltage drop due to the load effect and the droop effect. These problems were solved well by using RDC with extensive simulation validations. After addressing the issues of the power sharing and voltage regulation in one specific type of internal impedance, i.e., resistive impedance, a demand that operates inverters with different kinds of internal impedance arose. UDC came out as a result of the introduction of universal power transformation matrix and can be implemented well by RDC. In the grid-conned mode, an inverter usually needed a dedicated synchronization unit to synchronize its output voltage with the grid voltage. Although PLL was investigated deeply and utilized widely in modern electrical engineering, its nature of non-linearity increased the complexity of the control system and the parameters setting was always time-consuming. Thus, there was a need for removing the synchronization unit but keeping the synchronization function simultaneously. The operational mechanism of SUDC was explained, and its functionality of synchronization was verified fully and entirely by two simulations of an equivalent model.

To conclude, droop control and synchronization of single-phase inverter were analyzed thoroughly in this thesis from a simple controller to a sophisticated controller, from the stand-alone mode and to the grid-connected mode. Theoretical reasoning and realistic simulations were provided to support the analyses. However, there is still space left to improve the quality and depth of this thesis, e.g., choosing simulation parameters guided by control theory besides the trial and error method, finishing simulation of different operational modes for an inverter equipped with SUDC, and building hardware to obtain the hands-on and genuine understanding.

References

[1] U.S. Department of Energy, Clean Energy, Internet: https://www.energy.gov/science-innovation/clean-energy

[2] N. Mohan, T. M. Undeland, and W. P. Robbins. *Power Electronics: Converters, Applications, and Design.* John Wiley & Sons, 2003.

[3] Virginia Tech, Distributed Generation Educational Module, Internet: https://www.dg.history.vt.edu/index.html

[4] Wikipedia, Renewable Energy, Internet: https://en.wikipedia.org/wiki/Renewable_energy

[5] Q.-C. Zhong and T. Hornik. *Control of Power Inverters in Renewable Energy and Smart Grid Integration*. John Wiley & Sons, 2013.

[6] D. E. Olivares *et al.*, "Trends in Microgrid Control," *IEEE Trans. Smart Grid*, vol. 5, no. 4, pp. 1905-1919, Jul. 2014.

[7] Q.-C. Zhong, "Power-Electronics-Enabled Autonomous Power Systems: Architecture and Technical Routes," *IEEE Trans. Ind. Electron.*, vol. 64, no. 7, pp. 5907-5918, Jul. 2017.

[8] F. Blaabjerg, R. Teodorescu, M. Liserre and A. V. Timbus, "Overview of Control and Grid Synchronization for Distributed Power Generation Systems," *IEEE Trans. Ind. Electron.*, vol. 53, no. 5, pp. 1398-1409, Oct. 2006.

[9] X. Wang, J. M. Guerrero, F. Blaabjerg, and Z. Chen, "A Review of Power Electronics Based Microgrids," *Journal of Power Electronics*, vol. 12, no. 1, pp. 181–192, Jan. 2012.

[10] S. K. Sahoo, A. K. Sinha and N. K. Kishore, "Control Techniques in AC, DC, and Hybrid AC–DC Microgrid: A Review," in *IEEE Journal of Emerging and Selected Topics in Power Electronics*, vol. 6, no. 2, pp. 738-759, Jun. 2018.

[11] J. M. Guerrero, L. García de Vicuña, J. Matas, M. Castilla, and J. Miret, "Output impedance design of parallel-connected UPS inverters with wireless load-sharing control," *IEEE Trans. Ind. Electron.*, vol. 52, no. 4, pp. 1126–1135, Aug. 2005.

[12] J. M. Guerrero, J. Matas, L. García de Vicuña, M. Castilla, and J. Miret, "Wireless-Control Strategy for Parallel Operation of Distributed-Generation Inverters," *IEEE Trans. Ind. Electron.*, vol. 53, no. 5, pp. 1461–1470, Oct. 2006.

[13] J. M. Guerrero, J. Matas, L. García de Vicuña, M. Castilla, and J. Miret, "Decentralized Control for Parallel Operation of Distributed Generation Inverters Using Resistive Output Impedance," *IEEE Trans. Ind. Electron.*, vol. 54, no. 2, pp. 994–1004, Apr. 2007.

[14] J. M. Guerrero, L. Hang, and J. Uceda, "Control of Distributed Uninterruptible Power Supply Systems," *IEEE Trans. Ind. Electron.*, vol. 55, no. 8, pp. 2845–2859, Aug. 2008.

[15] J. M. Guerrero, J. C. Vasquez, J. Matas, L. G. de Vicuna and M. Castilla, "Hierarchical Control of Droop-Controlled AC and DC Microgrids—A General Approach Toward Standardization," *IEEE Trans. Ind. Electron.*, vol. 58, no. 1, pp. 158-172, Jan. 2011.

[16] J. M. Guerrero, M. Chandorkar, T. Lee and P. C. Loh, "Advanced Control Architectures for Intelligent Microgrids—Part I: Decentralized and Hierarchical Control," *IEEE Trans. Ind. Electron.*, vol. 60, no. 4, pp. 1254-1262, Apr. 2013.

[17] J. M. Guerrero, P. C. Loh, T. Lee and M. Chandorkar, "Advanced Control Architectures for Intelligent Microgrids—Part II: Power Quality, Energy Storage, and AC/DC Microgrids," *IEEE Trans. Ind. Electron.*, vol. 60, no. 4, pp. 1263-1270, Apr. 2013.

[18] Q.-C. Zhong and G. Weiss, "Synchronverters: Inverters That Mimic Synchronous Generators," *IEEE Trans. Ind. Electron.*, vol. 58, no. 4, pp. 1259–1267, Apr. 2011.
[19] Q.-C. Zhong, P.-L. Nguyen, Z. Ma, and W. Sheng, "Self-Synchronized Synchronverters: Inverters Without a Dedicated Synchronization Unit," *IEEE Trans. Power Electron.*, vol. 29, no. 2, pp. 617–630, Feb. 2014.
[20] Q.-C. Zhong, "Robust Droop Controller for Accurate Proportional Load Sharing Among Inverters Operated in Parallel," *IEEE Trans. Ind. Electron.*, vol. 60, no. 4, pp. 1281–1290, Apr. 2013.
[21] Q.-C. Zhong and Y. Zeng, "Universal Droop Control of Inverters With Different Types of Output Impedance," *IEEE Access*, vol. 4, pp. 702–712, Jan. 2016.
[22] Q.-C. Zhong and D. Boroyevich, "Structural Resemblance Between Droop Controllers and Phase-Locked Loops," *IEEE Access*, vol. 4, pp. 5733–5741, Sep. 2016.
[23] Q.-C. Zhong, W. L. Ming, and Y. Zeng, "Self-Synchronized Universal Droop Controller," *IEEE Access*, vol. 4, pp. 7145–7153, Oct. 2016.
[24] M. Karimi-Ghartemani, "Universal Integrated Synchronization and Control for Single-Phase DC/AC Converters," *IEEE Trans. Power Electron.*, vol. 30, no. 3, pp. 1544-1557, Mar. 2015.
[25] M. Ashabani, F. D. Freijedo, S. Golestan and J. M. Guerrero, "Inducverters: PLL-Less Converters With Auto-Synchronization and Emulated Inertia Capability," *IEEE Trans. Smart Grid*, vol. 7, no. 3, pp. 1660-1674, May 2016.
[26] K. D. Brabandere, B. Bolsens, J. V. den Keybus, A. Woyte, J. Driesen, and R. Belmans, "A Voltage and Frequency Droop Control Method for Parallel Inverters," *IEEE Trans. Power Electron.*, vol. 22, no. 4, pp. 1107–1115, Jul. 2007.
[27] A. Tuladhar, H. Jin, T. Unger, and K. Mauch, "Parallel operation of single phase inverter modules with no control interconnections," in *Proc. of APEC 97*, vol. 1, pp. 94–100, Feb. 1997.
[28] A. R. Bergen, and V. Vittal. *Power Systems Analysis*. Prentice Hall, 2000.
[29] Y. W. Li and C.-N. Kao, "An Accurate Power Control Strategy for Power-Electronics-Interfaced Distributed Generation Units Operating in a Low-Voltage Multibus Microgrid," *IEEE Trans. Power Electron.*, vol. 24, no. 12, pp. 2977–2988, Dec. 2009.
[30] Y. W. Li, D. Vilathgamuwa, and P. C. Loh, "Design, analysis, and real-time testing of a controller for multibus microgrid system," *IEEE Trans. Power Electron.*, vol. 19, no. 5, pp. 1195–1204, Sep. 2004.
[31] M. N. Marwali and A. Keyhani, "Control of distributed generation systems-Part I: Voltages and currents control," *IEEE Trans. Power Electron.*, vol. 19, no. 6, pp. 1541-1550, Nov. 2004.
[32] M. N. Marwali, J.-W. Jung, and A. Keyhani, "Control of distributed generation systems—Part II: Load sharing control," *IEEE Trans. Power Electron.*, vol. 19, no. 6, pp. 1551–1561, Nov. 2004.
[33] M. Dai, M. N. Marwali, J.-W. Jung, and A. Keyhani, "Power Flow Control of a Single Distributed Generation Unit," *IEEE Trans. Power Electron.*, vol. 23, no. 1, pp. 343–352, Jan. 2008.

[34] C. K. Alexander, and M. N. Sadiku. *Fundamentals of Electric Circuits*. McGraw-Hill Education, 2016.
[35] W. Yao, M. Chen, J. Matas, J. M. Guerrero, and Z.-M. Qian, "Design and Analysis of the Droop Control Method for Parallel Inverters Considering the Impact of the Complex Impedance on the Power Sharing," *IEEE Trans. Ind. Electron.*, vol. 58, no. 2, pp. 576-588, Feb. 2011.
[36] H. Bevrani and S. Shokoohi, "An Intelligent Droop Control for Simultaneous Voltage and Frequency Regulation in Islanded Microgrids," *IEEE Trans. Smart Grid*, vol. 4, no. 3, pp. 1505-1513, Sep. 2013.
[37] C. T. Chen. *Linear System Theory and Design*. Oxford University Press, 2012.
[38] Q.-C. Zhong and Y. Zeng, "Control of Inverters Via a Virtual Capacitor to Achieve Capacitive Output Impedance," *IEEE Trans. Power Electron.*, vol. 29, no. 10, pp. 5568-5578, Oct. 2014.
[39] Adel S. Sedra, and Kenneth C. Smith. *Microelectronic circuits: theory and applications*. Oxford University Press, 2017.
[40] R. W. Erickson, and D. Maksimovic. *Fundamentals of Power Electronics*. Springer, 2001.
[41] G. F. Franklin, J. D. Powell, and A. Emami-Naeini. *Feedback Control of Dynamic Systems*. Pearson Higher Education, 2010.
[42] R. E. Best. *Phase locked loops: design, simulation, and applications*. McGraw-Hill Professional, 2007.
[43] M. Karimi-Ghartemani and M. R. Iravani, "A new phase-locked loop (PLL) system," in *Proc. of 44th IEEE Midwest Symp. Circuits Syst. (MWSCAS)*, vol. 1, pp. 421-424, 2001.
[44] M. Karimi-Ghartemani and M. R. Iravani, "A nonlinear adaptive filter for online signal analysis in power systems: applications," *IEEE Trans. Power Del.*, vol. 17, no. 2, pp. 617-622, Apr. 2002.
[45] L. Harnefors, M. Bongiorno, and S. Lundberg, "Input-Admittance Calculation and Shaping for Controlled Voltage-Source Converters," *IEEE Trans. Ind. Electron.*, vol. 54, no. 6, pp. 3323–3334, Dec. 2007.
[46] D. Dong, B. Wen, D. Boroyevich, P. Mattavelli, and Y. Xue, "Analysis of Phase-Locked Loop Low-Frequency Stability in Three-Phase Grid-Connected Power Converters Considering Impedance Interactions," *IEEE Trans. Ind. Electron.*, vol. 62, no. 1, pp. 310-321, Jan. 2015.
[47] H. Akagi, E. H. Watanabe, and M. Aredes. *Instantaneous Power Theory and Applications to Power Conditioning*. John Wiley & Sons, 2017.

Appendix A Simulink Block Diagrams of RDC and CDC

The model initialization function for all cases in Chapter 3 is the same. The relevant MATLAB codes are:

```
Ts = 2e-6;              % Simulation step
Tsmp = 200e-6;          % Sample time
fg = 50;                % Grid frequency
Tg = 1/fg;
f = 7.5e3;              % Switching frequency
T = 1/f;
```

The module pictures and overall picture for two inverters equipped with RDC are as follows:

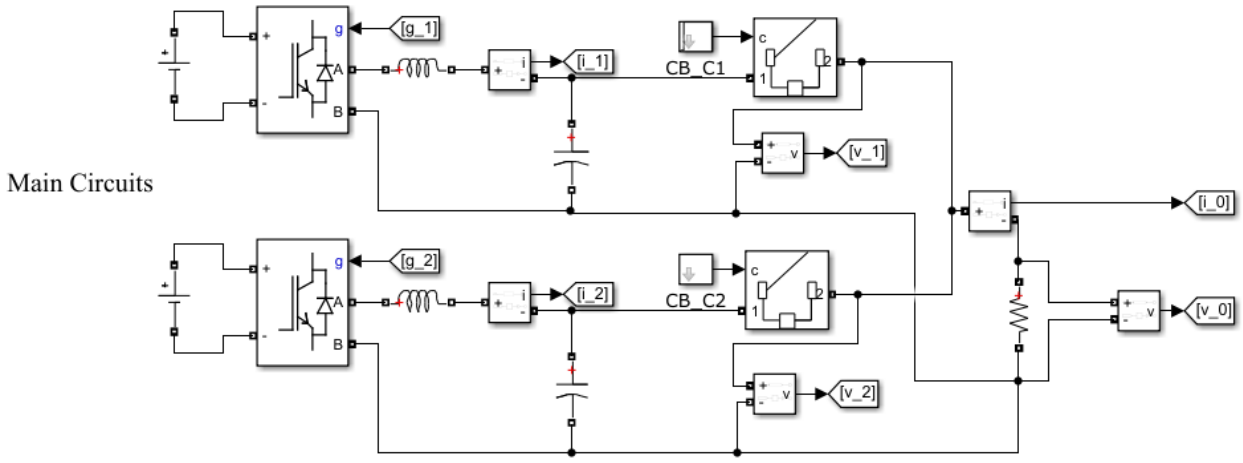

A.1: Main circuits of two inverters equipped with RDC.

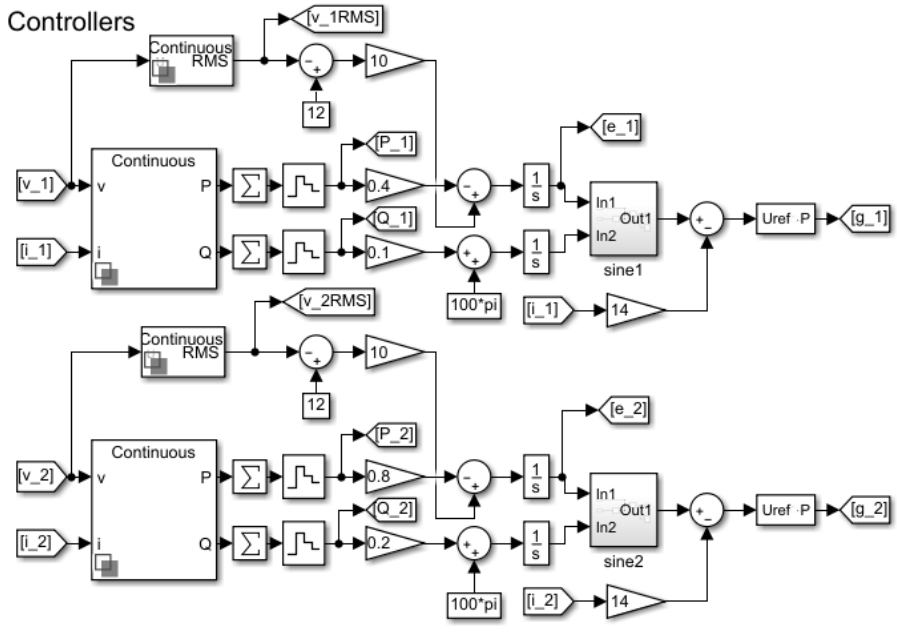

A.2: Controllers of two inverters equipped with RDC.

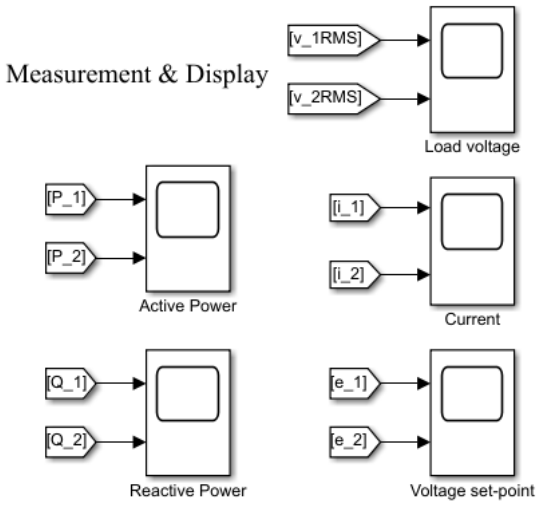

A.3: Measurement and display of two inverters equipped with RDC.

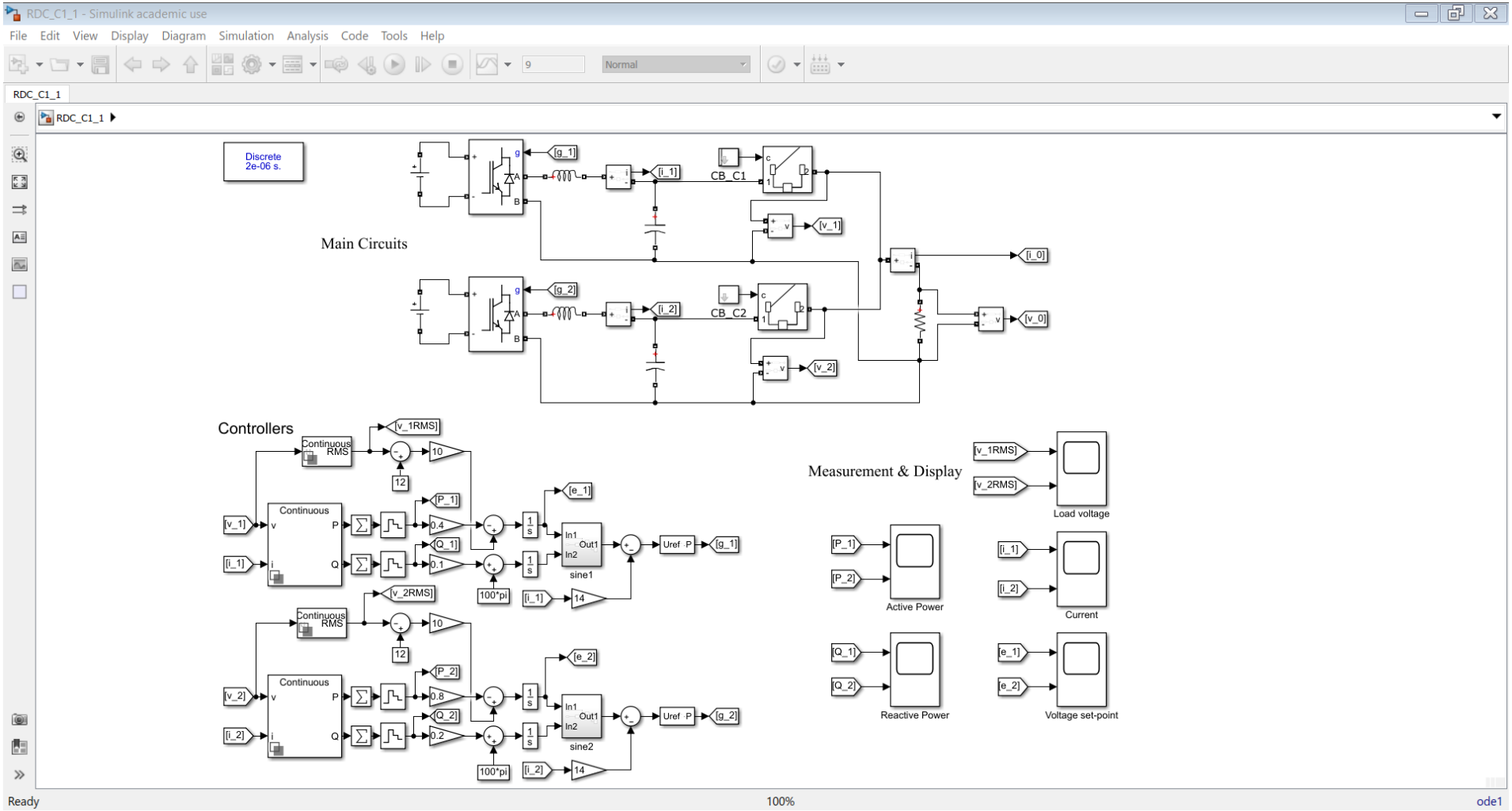

A.4: Overall picture of two inverters equipped with RDC.

The overall picture for two inverters equipped with CDC is as follows:

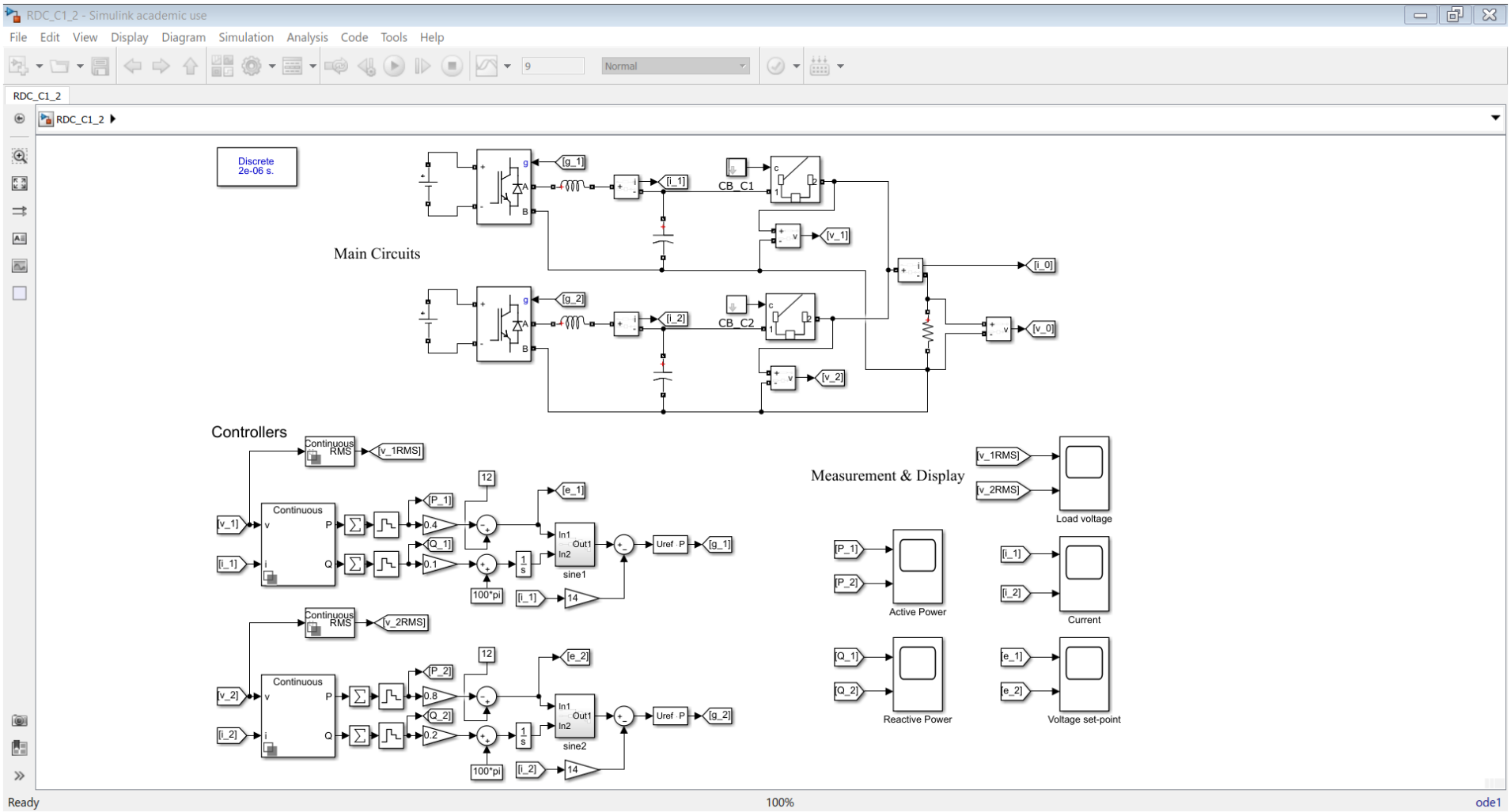

A.5: Overall picture of two inverters equipped with CDC.

Appendix B MATLAB Codes of UDC

The MATLAB codes for researching small-signal stability are as follows:

Characteristic Equation

```
% Parameters settings
% Variable
syms theta;
% Constants
omega = 10;
Z     = 8;
delta = 0;
m     = 0.48;
n     = 0.03;
E     = 12;
V     = 12;

% Characteristic coefficients
a = Z^2;
b = 2*omega*(Z^2);
c =
(omega^2)*(Z^2)+(cos(delta)*cos(theta)+sin(delta)*sin(theta
))*(m+n*E)*omega*V*Z;
d =
(cos(delta)*cos(theta)+sin(delta)*sin(theta))*(m+n*E)*(omeg
a^2)*V*Z;
e = m*n*(omega^2)*E*(V^2);

% Characteristic equation
f = a*(s^4)+b*(s^3)+c*(s^2)+d*s+e;
```

Real Parts of Roots

```
% Roots of characteristic equation
% Solutions
syms theta x;
f = 64*(x^4)+1280*(x^3)+((4032*cos(theta))/5 +
6400)*(x^2)+(8064*cos(theta))*x+2.4883e+03; %
Characteristic equation
s = solve(f,x);
% Roots
% s1 = - (100 - ((16257024*cos(theta)^2)/25 -
3185024/5)^(1/2)/32 - (126*cos(theta))/5)^(1/2)/2 - 5;
% s2 = (100 - ((16257024*cos(theta)^2)/25 -
3185024/5)^(1/2)/32 - (126*cos(theta))/5)^(1/2)/2 - 5;
% s3 = - (((16257024*cos(theta)^2)/25 - 3185024/5)^(1/2)/32
- (126*cos(theta))/5 + 100)^(1/2)/2 - 5;
% s4 = (((16257024*cos(theta)^2)/25 - 3185024/5)^(1/2)/32 -
(126*cos(theta))/5 + 100)^(1/2)/2 - 5;

% Calculations
k1=0;
for theta = -pi/2: pi/360: pi/2
    k1=k1+1;
    s1(k1) = - (100 - ((16257024*cos(theta)^2)/25 -
3185024/5)^(1/2)/32 - (126*cos(theta))/5)^(1/2)/2 - 5;
end

k2=0;
for theta = -pi/2: pi/360: pi/2
    k2=k2+1;
    s2(k2) = (100 - ((16257024*cos(theta)^2)/25 -
3185024/5)^(1/2)/32 - (126*cos(theta))/5)^(1/2)/2 - 5;
end

k3=0;
for theta = -pi/2: pi/360: pi/2
    k3=k3+1;
    s3(k3) = - (((16257024*cos(theta)^2)/25 -
3185024/5)^(1/2)/32 - (126*cos(theta))/5 + 100)^(1/2)/2 -
5;
end
```

```
k4=0;
for theta = -pi/2: pi/360: pi/2
    k4=k4+1;
    s4(k4) = (((16257024*cos(theta)^2)/25 -
3185024/5)^(1/2)/32 - (126*cos(theta))/5 + 100)^(1/2)/2 -
5;
end

figure;
plot(-pi/2: pi/360: pi/2, s1, 'r'); grid on; hold on;
plot(-pi/2: pi/360: pi/2, s2, 'b--');hold on;
plot(-pi/2: pi/360: pi/2, s3, 'y-.');hold on;
plot(-pi/2: pi/360: pi/2, s4, 'm:');hold on;
xlabel('Angle (rad)'); ylabel('Real parts of roots');
legend('s1','s2','s3','s4');axis([-2 2 -12 4]);
```

Routh's Stability

```
% Parameters settings
% Variable
syms theta;
% Constants
omega = 10;
Z     = 8;
delta = 0;
m     = 0.48;
n     = 0.03;
E     = 12;
V     = 12;

% Characteristic coefficients
a = Z^2;
b = 2*omega*(Z^2);
c =
(omega^2)*(Z^2)+(cos(delta)*cos(theta)+sin(delta)*sin(theta
))*(m+n*E)*omega*V*Z;
d =
(cos(delta)*cos(theta)+sin(delta)*sin(theta))*(m+n*E)*(omeg
a^2)*V*Z;
e = m*n*(omega^2)*E*(V^2);

% Routh coefficients
A = (b*c-a*d)/b;
B = d-(b^3)*e/((b*c-a*d)*d);

% Calculations
j=0;
for theta = -pi/2: pi/360: pi/2
    j=j+1;
    A(j) = ((2016*cos(theta))/5 + 6400);
end

k=0;
for theta = -pi/2: pi/360: pi/2
    k=k+1;
    B(k) = (8064*cos(theta) -
4529848320/(7*cos(theta)*(516096*cos(theta) + 8192000)));
end
```

```
figure;
plot(-pi/2: pi/360: pi/2, A, 'r'); grid on; hold on;
plot(-pi/2: pi/360: pi/2, B, 'b--');
xlabel('Angle (rad)'); ylabel('Amplitude');
legend('A','B'); axis([-2 2 -10000 10000]);
```

Appendix C Simulink Block Diagrams of SUDC

The module pictures and overall picture of the inverter equipped with SUDC are as follows:

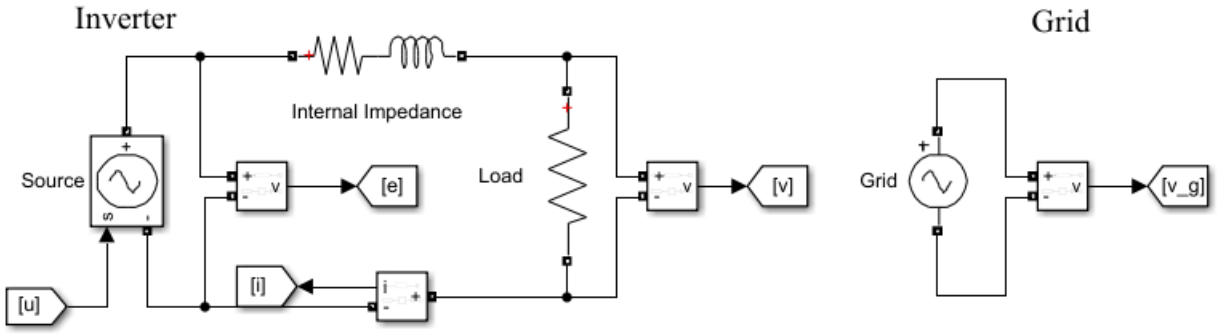

C.1: Inverter and grid of the inverter equipped with SUDC.

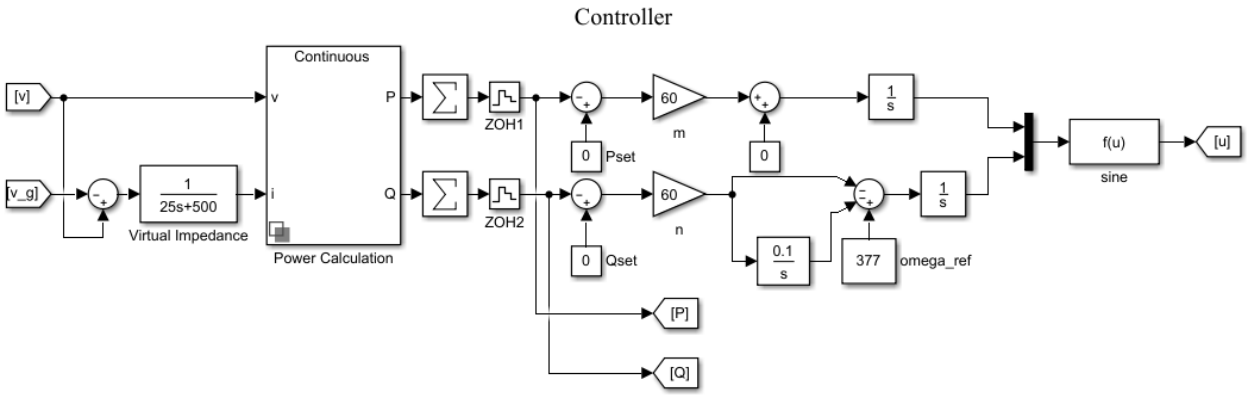

C.2: Controller of the inverter equipped with SUDC.

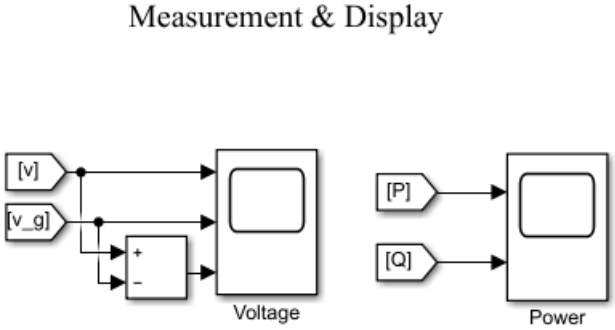

C.3: Measurement and display of the inverter equipped with SUDC.

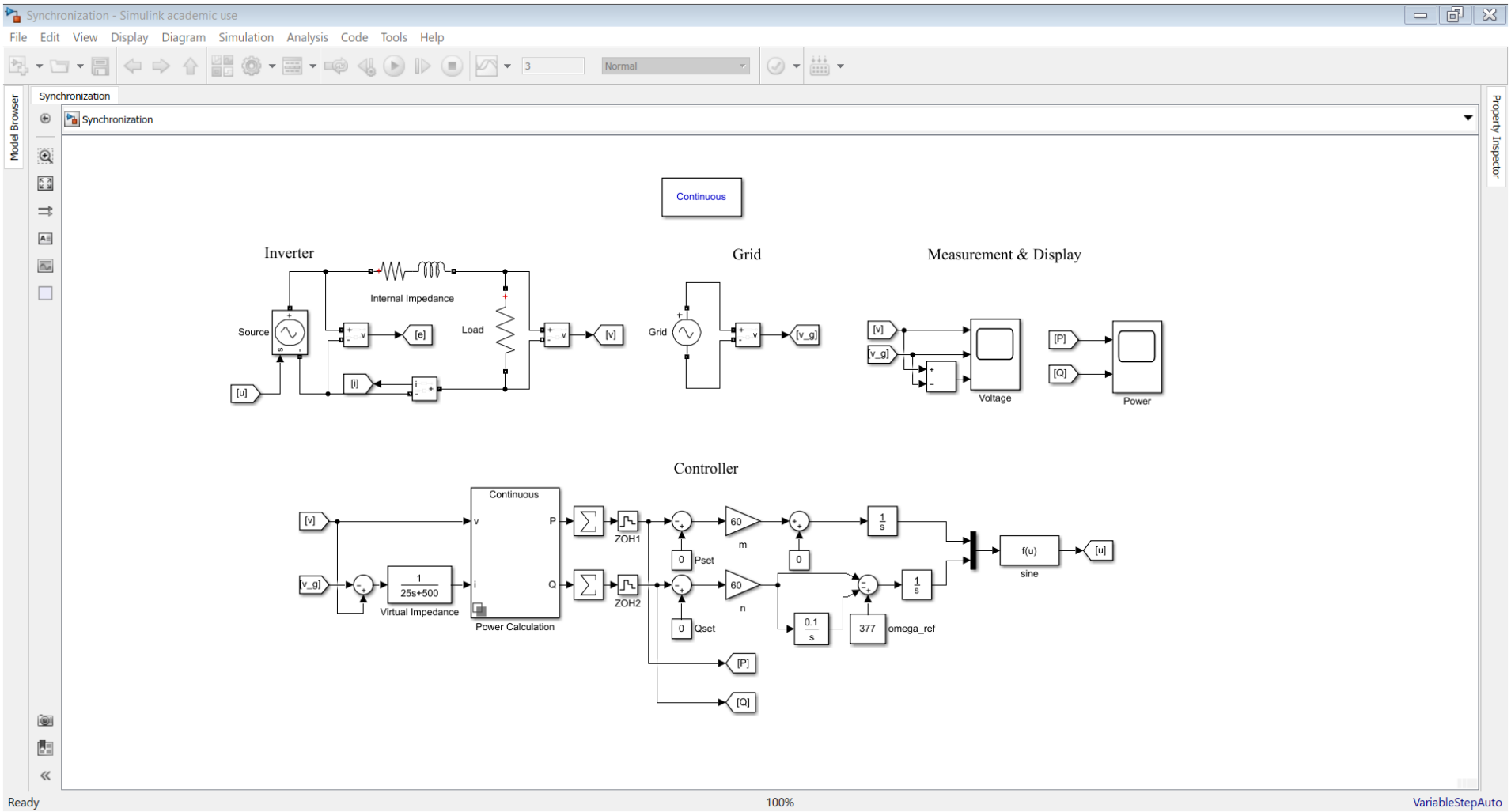

C.4: Overall picture of the inverter equipped with SUDC.